Evaluation of New Bone Formation in Rabbit Calvarial Defects Induced by Silk Fibroin Scaffolds Coated with Fibronectin and Decellularized Dental Pulp

Thanh Huy Thai

A Thesis Submitted in Fulfillment of the Requirements for the Degree of

Master of Science in Oral and Maxillofacial Surgery

Prince of Songkla University

2016

Thesis Title	Evaluation of New Bone Formation in Rabbit Calvarial Defects Induced by Silk Fibroin Scaffolds Coated with Fibronectin and Decellularized Dental Pulp
Author	Mr. Thanh Huy Thai
Major Program	Oral and Maxillofacial Surgery

Major Advisor :

……..

(Assoc .Prof. Thongchai Nuntanaranont)

Co-advisor

…….……..

(Asst. Prof. Dr. Jirut Meesane)

…….……..

(Assoc. Prof. Dr. Suttatip Komolmatyakol)

Examining Committee :

…….……..Chairperson

(Assoc. Prof. Dr. Somchai Sessirisombat)

……..

(Assoc .Prof. Thongchai Nuntanaranont)

……..……..

(Assoc. Prof. Dr. Suttatip Kamolmatyakul)

……

(Asst. Prof. Dr. Jirut Meesane)

The Graduate School, Prince of Songkla University, has approved this thesis as partial fulfillment of the requirements for the Master of Science Degree in Oral and Maxillofacial Surgery.

……..……..

(Assoc. Prof. Dr. Teerapol Srichana)

Dean of Graduate School

This is to certify that the work submitted is the result of the candidate's own investigations. Due acknowledgement has been made of any assistance received.

……...……

(Assoc. Prof. Thongchai Nuntanaranont)

Major advisor

……...……

(Mr. Thanh Huy Thai)

Candidate

I hereby to certify that this work has not been accepted in substance for any degree, and is not being currently submitted in candidature for any degree.

……

(Mr. Thanh Huy Thai)

Candidate

Thesis Title	Evaluation of New Bone Formation in Rabbit Calvarial Defects Induced by Silk Fibroin Scaffolds Coated with Fibronectin and Decellularized Dental Pulp
Author	Mr. Thanh Huy Thai
Major Program	Oral and Maxillofacial Surgery
Academic Year	2016

Abstract

Objective: This study aimed to evaluate the silk fibroin scaffolds coated with fibronectin and decellularized dental pulp enhancing new bone formation in the rabbits' calvarial defects.

Materials and Methods: The 3D porous silk fibroin (SF) scaffolds were fabricated and coated by fibronectin and decellularized dental pulp. Observation of the coated SF scaffolds' morphologic surfaces by SEM before experiment. The 36 bilateral bicortical calvarial defects of the 18 rabbits were used, they were divided into three groups randomly: SF, silk fibroin scaffold coated with fibronectin and decellularized dental pulp scaffolds (SF-FP), and autogenous bone graft (AB) as control group. The rabbits were sacrificed at 2, 4, 8 weeks postoperative. The morphology surfaces of the scaffolds, and the new bone formation, inflammation, vascularization of the experiments were evaluated by SEM, radiograph, micro-CT, and histology.

Results: The SF-FP scaffolds had high porosity, and their pore sizes were smaller than the SF scaffolds significantly ($p<0.001$). All experimental rabbits were good recovery, no evidence of infection or dehiscence. The SF-FP implants were enhanced new bone formation better than in the SF implants *in vivo* experiment. Moreover, the SF-FP implants were lesser inflammation, more vascularization, and slower degradation than in the SF implants.

Conclusion: The present study showed that the silk fibroin scaffolds coated with fibronectin and decellularized dental pulp enhanced new bone formation. They had the

properties of osteoconduction, biocompatibility, and biodegradability. The SF-FP scaffold promises to use as a novel bone scaffold for bone tissue engineering.

Acknowledgement

I am, as always, sincerely grateful to my supervisors, Assoc. Prof. Thongchai Nuntanaranont, Asst. Prof. Jirut Meesane, and Assoc. Prof. Suttatip Kamolmatyakul, who gave me the opportunity to study from their valuable knowledge and experiences throughout this training time.

I deeply thank to Mr. Jakchai Jantaramano and Ms. Supaporn Sangkert who helped and advised me throughout this study. I would like thank to research staff of the Dental Research Center who guided me using equipment's research in the study. I also thank to the staff in Animal House, Faculty of Science who cared my animals in the study.

I honestly thank to Dr. Sukhum Keerativitayanun for his supporting of the accommodation. I would like to thank Assoc. Prof. Pichai Vittayakittipong, Assoc. Prof. Prisana Pripatnanont, Asst. Prof. Settakorn Pongpanich, and OMFS staff, OR staff, OMFS staff of Trang Hospital and Orthodontics staff, who helped and gave me many beautiful memories.

I would like to thank Ms. Benjawan Triranurat for her kind help. I also thank to Mr. Mitch Atkins and my nice friends at OMFS, Orthodontics, and Prosthodontics, who helped me by many various ways.

I would like to thank the committee of Thailand's Education Hub for Southern Region of ASEAN Countries (TEH-AC) Scholarship, Graduate school, Prince of Songkla University for financial supporting in my study.

Finally, nothing I do comes without my warmhearted thanks to my wife or my best friend, Ha,our daughter, and our parents for their unconditional love and never-ending support.

Thanh Huy Thai

Contents

List of the Tables

List of Figures

List of Abbreviations and Symbols

% BV/TV	=	Percentage of bone volume per total volume fraction
µA	=	Microampere
µm	=	Micrometer
μm^3	=	Cubic micrometer
3D	=	Three dimensions
AB	=	Autogenous bone
BMPs	=	Bone morphology proteins
BVF	=	Bone volume fraction
DMEM	=	Dulbecco modified Eagle's Media
ccm	=	Cubic centimeter
ECM	=	Extracellular matrix
EDTA	=	Ethylenediaminetetraacetic acid
FBS	=	Fetal bovine serum
FN	=	Fibronectin
GAGs	=	Glycosaminoglycans
H	=	Host bone
H&E	=	Haematoxylin and Eosin
kg	=	kilogram
L	=	Left side
micro-CT	=	micro computerized tomography
MMPs	=	metalloproteinase
MPa	=	Megapascal
MW	=	Megawatt
NB	=	New bone
OD	=	Optical Density
PCL	=	Polycaprolactone
PLA	=	Poly (L-lactic acid)
PLGA	=	Poly L-lactide-co-glycoside
PMMA	=	Polymethylmethacrylate

List of Abbreviations and Symbols (cont.)

R	=	Right side
REC	=	Research Ethics Committee
RGD	=	Arg-Gly-Asp
rpm	=	round per minute
SD	=	Standard Deviation
SEM	=	Scanning Electron Morphology
SF	=	Silk fibroin scaffold
SF-FP	=	Coated silk fibroin scaffold with fibronectin and decellularized dental pulp
TE	=	Tissue engineering
TGF- β	=	Transforming growth factor-beta
UTS	=	Ultimate tensile strength
w/v	=	weight/volume

Chapter 1

Introduction

Background and Rationale

Nowadays, many patients have bone loss problems in oral and maxillofacial region, such as trauma, periodontal diseases, and bone resoption that affects their functions, esthetics, and quality of life. Bone graft reconstructive surgery is necessary to reconstruct the bone loss problems in all three dimensions. The mechanism of bone graft healing and bone regeneration includes three processes are osteoconduction, osteoinduction, and osteogenicity. The bone graft materials need to have at least one of three characteristics to improve bone healing. There are two main bone graft types for bone regeneration such as autogenous bone graft and allogenous bone graft. The autogenous bone graft which is harvested from another site of individual own body is considered as the gold standard of bone transplantation. However, its usage is limited by secondary operation, pain, blood loss, and supply, etc. Furthermore, the allogenous bone graft which is harvested from cadavers' bone has its limitations such as immunogenic response and disease transmission [1]. Tissue engineering (TE) is a promising solution to treat the bone loss problems. The TE approaches involve regenerating a tissue within the suitable scaffolds which are constructed as same as a target tissue. A functional tissue regeneration needs a mimicked microenvironment for preferring cells reaction [2, 3]. As a result, this alternative treatment may overcome the limitations of the current bone graft therapies [2, 4].

The scaffold of the bone regeneration should have osteoconductive property to remote important bone cells as osteoblasts and osteoprognitor cells that would able to adhere, to migrate, to differentiate cells on the scaffold, and to synthesize a new bone matrix [5]. Properly the scaffolds would be designed the size and structure for potential applications in TE [4].

Silk fibers are a biological material in nature. The main characteristic of silk fibers is proteins which are applied as sutures and haemostatic drug delivery agents [6]. Silk fibroin scaffold is fabricated from silk fibers. The main composition of silk fibroin is unique β-sheet (crystalline)-rich structure which is high stiffness and toughness. It roles as the useful biopolymer for bone engineering applications [7]. The applications of silk-based scaffolds in engineering are various types of tissues, such as (a) hard tissue, e.g., bone, cartilage; (b) soft tissue, e.g., ligaments, vascular, nervous tissue; (c) organ, e.g., ear, bladder, skin, ect [6]. The combination of silk fibroin scaffolds and other components, such as RGD sequence of fibronectin, platelet-rich fibrin (PRF), not only increase biocompatibility of silk, but also improve osteoconduction in bone TE [6-10].

Fibronectin is an extracellular matrix (ECM) glycoprotein which has cell friendly characteristic. The fibronectin is assembled into a fibrillar matrix in all living tissue. It is used to coat synthetic scaffold materials to promote biocompatibility of biomaterials [11]. Moreover, it interfaces with cells and orders cell functions, e.g. cells adhesion, cells growth, and cells differentiation [12]. The silk fibroin scaffolds increase cells attachment when they are combine with fibronectin. The combination improves the silk scaffold to decrease inflammatory reaction and to enhance vascularization [9, 13].

The decellularization approaches aim to exclude cells from their ECM that remove antigens of inflammatory reaction or implants rejection. Moreove, they aim to collect the extracellular matrix (ECM) which covers all cells, tissue and organs. The ECM has many essential components for affecting cell functions directly, such as collagens, fibronectin, laminin, glycosaminoglycans, and growth factors. Moreover, it is used as the biological scaffolds which are applied in surgical reconstruction, tissue engineering, and organ transplantation [11, 14, 15]. The quaternary structure of proteins of the ECM is necessary for xenogeneic ECM to play as a biological scaffold rather than promote an inflammatory response [11]. The proteins of ECM which attach on scaffolds' microenvironment can enhance cell growth and differentiation [16]. Besides that, the ECM of human dental pulp has many components which are essential

for bonr tissue engineering such as collagens (type I, III); glycoprotein, e.g., fibronectin, bone sialoprotein, hyaluronic acid; and growth factor, e.g., bone morphology proteins (BMPs) [17]. The combination of silk fibroin scaffold and decellularized dental pulp enhances the artificial fibril matrix which encourages cells adhesion, migration, and differentiation [18].

The combination of fibronectin, decellularized dental pulp, and collagen enhances the silk fibroin scaffolds' properties that improve quality of cell adhesion, differentiation, proliferation *in vitro*. The silk fibroin scaffolds coated with multiple components may potential material in bone tissue engineering application [18]. Furthermore, no article investigates the potential biomaterial of the silk fibroin scaffolds coated with fibronectin and decellularized dental pulp in bone regeneration or did not evaluate inflammatory reaction, new bone formation of the coated scaffolds in vivo experiment.

This study aimed to evaluate new bone formation property of the silk fibroin scaffolds coated with fibronectin and decellularized dental pulp *in vivo* experiment.

Literatures review

Bone regeneration and materials

All bone materials which are applied in bone reconstructive surgery need to associate at least one of three basic mechanical functions, such as osteoconduction, osteoinduction, and osteogenesis. This bone healing mechanism leads to bone regeneration successfully [2].

Osteoconduction is a structural property of bone graft function that is necessary to provide a suitable scaffold for bone cells attachment properly. The scaffold is able to enhance osteoblasts, vessels which attach on it to regenerate new bone tissue [19]. The design of the scaffold should have proper properties which are porous sizes, interconnective pores, and surfaces enhance cells adhesion, growth factors releasing inside the scaffold [20].

Osteoinduction is the property that stem cells are able to recruit into the grafting scaffold. Then they are able to differentiate into osteoblasts. Moreover, many growth factors influence the process, such as platelet-derived growth factors, bone morphogenesis proteins (BMPs), insulin-like growth factors (I and II), transformer growth factor-β (β_1 and β_2), vascular endothelial growth factor (VEGF), etc. [19, 20].

Osteogenesis is the process of new bone formation. It is natural bone growth, bone repair. It occurs when the possible osteoblasts and osteoclast precursors are able to replace the bone graft material [19, 20].

Types of bone grafting

Bone-grafting materials need to have at least one of the properties, such as osteoconduction, osteoinduction, and osteogenesis. There are three primarily groups of bone graft material, such as autogenous bone, allogeneic bone, and alloplastic bone which substitutes are xenograft and tissue-engineering materials [1].

Autogenous bone is harvested from another site of individual own body, such as iliac crest, tibia prominent, mandibular symphysis, etc. Currently autogenous bone graft or autologous bone is considered as the gold standard of bone graft material. Because the autogenous bone graft have all three properties of bone healing mechanism, does not trigger immunogenic response, and has osteogenic cells in bone graft material. However, it still maintains many disadvantages, such as secondary operative sites, limited amount, blood loss, pain, donor site morbidity, ect [1].

Allogenous bone graft that is harvested from cadavers' bone can be an alternative for autogenous bone graft's limitations. For example, it has amount of bone, reducing operation sites and donor site morbidity. Mostly the forms of bone allograft are frozen, mineralized free-dried, demineralized free-dried and irradiated bone. The mineral free-dried bone is able to form bone by osteoconduction and osteoinduction. The allogenous bone graft does not have osteogenic cells as same as autogenous bone graft. Thus, it takes longer time for bone formation, and improves less bone formation volume than autogenous bone graft. Moreover, it still remains

disadvantages, e.g. familiarizing possibilities of immune rejection and pathogen transmission or infection [1].

Alloplast bone graft is artificial material from animals' bone or artificial bone materials that overcome a large of disadvantages of autogenous and allogenous grafts. The alloplast graft which is produced to osteoconductive function is a framework for cells recruitment, adhesion, differentiation, and proliferation. It can be combined with mesenchymal stem cell as own osteoinductive to stimulate regenerative process. It is highly available in amount, sizes, textures, shapes, and porosity flexible [1].

Tissue engineering

Tissue engineering is defined by Langer and Vacanti [3], tissue engineering is "an interdisciplinary field that applies the principles of engineering and life sciences toward the development of biological substitutes that restore, maintain, or improve tissue function or a whole organ". Tissue engineering relates with cell attachment within a scaffold. The scaffold needs to provide a proper structure which supports for the cell functions. Additionally, the scaffold surface has topography and chemistry (wettability, softness and stiffness, roughness); structure (porosity, pore size, pore shape, interconnectivity, specific surface area) and mechanical properties that encourage cells performances and activities for tissue regeneration applications such as peripheral nerves, skin, cartilage [21]. Many tissue engineering materials are for medical application from different origins, such as metal origin, e.g. titanium implants, titanium mesh; ceramic origin, e.g. calcium phosphate, bioactive glass, calcium sulfate; synthetic origin, e.g. polycaprolactone, polymethylmethacrylate; and natural origin, e.g. silk fibroin, chitosan, collagen, fibrin [2].

Scaffolds for bone tissue engineering

3D porous scaffolds offer a suitable microenvironment for TE. They may be added stem cells with or without growth factors to stimulate their biofunctionality. A suitable scaffold needs to have following properties generally in

TE, including biocompatibility, biodegradability, mechanical properties, architecture designs, and manufacturing technology [21].

Biocompatibility is an important criterion of a scaffold for tissue engineering purpose. The scaffold must be minor immune response to avoid serious inflammation that may decrease wound healing or increase implant rejection [21]. For example, silks are a non-immunological material after purification. The silk fibroin scaffolds are fabricated properly to improve biocompatibility. Moreover, they are fewer inflammatory response than poly (L-lactide-co-glycoside) (PLGA) scaffolds and collagen [22].

Biodegradability is that the TE materials accept the own cells to interchange from the implanted scaffold to target tissue regeneration finally. Therefore, the scaffold must be biodegradable that allows to produce their own extracellular matrix of cells. The scaffolds should be able to exit host body without affecting other organs. The proper inflammatory response is necessary for biodegradability of scaffolds [21]. Silk fibroin scaffold can enhance for cell growing to regenerate new bone tissue, then it is biodegradable within a time frame of 1–2 years *in vivo* [13].

Mechanical properties of a scaffold are very important. The scaffold should be durable and efficient enough to perform surgical procedure throughout implantation, such as in engineer bone, vascula, etc. The scaffold should have steady similar as the anatomical site which need to be replaced [21]. For example, the scaffolds are fabricated mechanical properties properly that is a challenge in bone tissue engineering. Silk is a superior toughness which is high performance biomaterial in bone TE [23]. The potentiality of the silk fibroin porous scaffold for bone and cartilage repairs has been proved by many experimental results [8, 23].

Architecture of scaffolds is very important for tissue engineering. The 3D scaffold must have a interconnective pore arrangement which enhance cells entrance [21]. For example, osteoblast was found to migrate faster inside the larger pore of microcellular poly HIPE scaffolds, approximately 100 μm [24]. Besides that, a

scaffold's surface may be hydrophobic or hydrophilic, that are non-wetting bacteriological dishes and wettable tissue culture dishes, respectively. Hydrophobicity is key factor to cell response. The surface is able to evaluate by contact angle which is correlation with hydrophobicity, e.g. reversible correlation with hydrophilic surface. The hydrophilic surface enhances more cell attachment [25]. However, it does not produce much cells attachment if the hydrophilic rate is very high. Thus, the hydrophobicity also associates with cell delivery and development [26].

Inclusion, the tissue engineering has the important role in life science forwarding development of biological substitutes to improve organ function. The 3D construct scaffold with many essential properties which active as TE scaffold properly.

Silk fibroin material

Silk fibroin scaffold

Silk-based materials are prepared from *Bombyx mori* silkworm silk or mulberry silk [6]. Silk fibroin not only is used as surgical sutures for a long time, but also has many benefits in biomaterials, such as low risk of infection, not expensive, high production. The bioactive properties of silk fibroin are flexibility, strength, biocompatibility and biodegradability that are necessary for bone regeneration [6, 23]. The application of silk-based scaffolds in engineering various types of tissues, as (a) hard tissue, e.g., bone, cartilage; (b) soft tissue, e.g., ligaments, vascular, nervous tissue; (c) organ, e.g., ear, bladder, skin, ect [6].

There are several important properties for serving as a good biomaterial. Firstly, they are good mechanical toughness, self-assembly, processing flexibility. Secondly, they have the biocompatibility, non-inflammation, non-cytotoxicity, and lower antigenicity than other biodegradable polymers. In addition, their properties are the process ability into different morphological forms with controllable porosity, and regulation of the structure and morphology in all aqueous process. Finally, their degradation rate can be adjusted to regulate the release of the bioactive molecule; oxygen and water permeability [6, 8, 23, 27, 28].

Mechanical properties

The *Bombyx mori* silk fibroin was chosen because of its desirable properties, such as biocompatibility with low inflammatory and immunogenic response [7, 23, 29-31]. The silk from the cocoon of B. mori contains primarily of three proteins, which consists of the glue-like glycol sericin protein, and light and heavy chains of fibroin with 26 and 390 kDa, respectively. The sericin which coats outside of the fibroin cores is a glue-like protein [22, 32]. The heavy-chain fibroin is necessary for bone tissue engineering, but the presence of the glycoprotein sericin is the cause of inflammation reaction [33]. Thus, the sericin is extracted necessarily to improve the biocompatibility of silk material for bone tissue engineering.

The unique β-sheet (crystalline)-rich structure of silk fibroin is reported as a high toughness which make silk as a strong biopolymer for bone regeneration [7, 23, 34]. The β-sheet hydrophobic copolymer blocks are connected by small random coils which are hydrophilic linker sections. The β-sheet protein of silk fibroin is reverse connection with glycine-X repeats component that X is alanine, threonine, serine, or valine. Moreover, these domains have subdomain within them, such as glycine, serine, alanine, and tyrosine [32]. Therefore, these modules of cloned silk importantly simulate the native properties [23]. By management of these structures, the silk fibroin degradation rate may be adjusted possibility [31]. Additionally the hydrophobic fibroin of silk can arrange itself by β-sheet-forming regimens to establish resilient and durable materials. The silk fibers' toughness is higher than Kevlar [23]. Moreover, they are stronger than poly (L-lactic acid) (PLA) or collagen which are polymeric degradable biomaterials. The ultimate tensile strengths (UTS) of PLA and collagen are lower than the silk fibers at 50 MPa, 7.4 MPa, and 740 MPa, respectively [22]. That makes silk fibroin is an excellent polymer for tissue regeneration, such as bone, cartilage, or tendon.

Biocompatibility of silk fibroin scaffolds

As others biomaterials, silk may provoke some unfavorable foreign-body reaction that cannot exclude from silk proteins [6]. The sericin which is known as the antigenic characteristic of silk is the glue-like protein cover silk fibers. The

sericin can be rejected by silk purification protocol that decrease the antigenic effects of silk [35]. In a study of Wang, the silk scaffolds produced mild immune and inflammatory reaction for one year; the overall appearance of immune response such as IFN-δ, TNF-α, IL (4, 6, and 13) that could not be detected in the silk fibroin scaffolds [31]. Moreover, inflammatory response of silk fibroin films was minimal after six weeks implantation. The interface layer was detected rare lymphocytes and no foreign-body giant cells. These films were positive response from host bone with mild inflammation, good compact zone and good tissue regeneration that are better than PLA or collagen films [35].

Biodegradability of silk fibroin scaffolds

Biodegradation, in term, is used that the molecular weight of polymer constructing the material is reduced over time by enzymatic biological action. The biomaterials are degraded slowly that can maintain tissue integrity following implantation while continually transferring the load-bearing burden to the developing biological functional tissue [27]. Silk fibroin is a biodegradable natural polymer. Silk fibroin can be catalytically hydrolyzed by acids, alkalis, salts, and proteases. Silk fibroin is gradually degraded into low molecular weight peptides during the hydrolysis process, and further hydrolyzed into free amino acid [36]. Silk fibroin fibers retain more than 50% of their mechanical properties after two months of implantation, lose the majority of their tensile strength within one year, and fail to recognized at the site after two years *in vivo* [22].

The biodegradation of silk fibroin is evaluated generally by accessing the effects of proteases on the structure, property changes of silk fibroin, and the influences of the structure of silk fibroin material on the degradation rate. The protein cocktails such as collagenase, α-chymotrypsin are aptitude-degrading silk into free amino acid [22, 27]. In vitro, protease XIV from Streptomyces griseous is widely used as model enzyme for silk, and it is followed by α-chymotrypsin [6, 37]. Additionally, the degradation of silk is shown that osteoblasts and osteoclast cells could corrode silk films by expression of metalloproteinase (MMPs) *in vitro*. These results are inspiring

because native extracellular matrix is remodeled *in vivo* continuously by synchronous proteolytic degradation via MMPs [6].

In summary, *in vivo* silk fibroin is non-cytotoxicity materials, good mechanical properties, and degradable products. Furthermore, its biocompatibility and degradatibility mechanisms are useful to fabricate silk-based materials with non-cytotoxicity, predictable biodegradability, and mechanical properties in bone TE [37].

Fibronectin

Property of Fibronectin

Fibronectin (FN) is present in both plasma and cells. The hepatocytes of liver synthesize plasma fibronectin with 300 mg/ml concentration in blood plasma. Besides that, fibroblasts and multiple other cell types secrete cellular fibronectin which is arranged into fibrils within extracellular matrix. The amount of fibronectin is only lower than collagen in ECM. It is widely expressed with a high molecular weight dimeric glycoprotein (~450 kDa per dimer). FN has three types of modular protein: 12 type I, 2 type II, and 15- 17 type III repeating unit [12]. FN presents in all ECM structures, such as submucosa, interstitial tissue and membranes. The cell-friend properties of FN encourage attracting cells that may apply to coat many scaffold materials to enhance biocompatibility [11, 38]. The Arg-Gly-Asp (RGD) subunits which are necessary for cell adhesion are rich in FN. FN exists within ECM at early stage of embryos development that is important for growing vascula and human structures [38, 39]. FN is very important in regarding cell–matrix communication [11]. Fibronectin is enriched in the early wound bed, migrated a number of mesenchymal cell types *in vivo* [39].

Fibronectin and cells adhesion

Fibronectin is formed into a cell surface’s fibrillar network via interaction of cell surface receptors that orders many functions of cells, such as cell adhesion, migration, growth, and differentiation [12]. For example, fibronectin on cells seeded on collagen- and fibronectin-coated dishes that induced cell growth. Moreover, addition of soluble fibronectin to cells seeded on laminin-coated dishes

resulted in a 5-fold increase in cell growth [40]. The attachment and proliferation of BALB/3T3 mouse fibroblasts were improved significantly on films made of the RGD modified silk proteins [9]. The osteoblast-like cells (Saos-2) significantly attached to RGD-silk films. The fibronectin revealed an alteration of hydrophobicity and stimulated mineralization of osteoblast *in vitro*. The RGD- silk fiber matrixes could support mesenchymal stem cells adhesion and spread collagen type I formation [41]. Besides that, the dental implants coated with fibronectin enhanced osseointegration around dental implant in rabbits [42]. The fibronectin coating on scaffold not only attract cells, but also spread and proliferate these cells.

Decellularized Dental Pulp

Decellularization method

The decellularization methods target to remove cells from their ECM. Therefore, they exclude possible antigens which may trigger inflammatory reaction or reject implants. There are many different procedures of decellularization. The proper procedure is chosen depending on cell and matrix density, tissue, organ morphology. Physical treatments which are agitation, mechanical pressure, sonication, or freeze-thawing procedures interrupt the membrane of cells. Commonly the physical treatments are combined with chemical process with detergents to. A variety of the decellularized method is enzymatic treatment by trypsin, esterases, dispase, or nucleases. Currently the hydrostatic pressure, detergent, and enzymatic procedures are investigated *in vivo*. The decellularized ECM can maintain its 3D porous ECM scaffold which mostly compose of collagen fibers [43].

Background of Extracellular Matrix

The extracellular matrix (ECM) biological scaffolds are applied in alternative surgical reconstruction commonly. They are also used in biomedical regeneration or organ transplantation. The ECM represents all cells of each tissue and organ, and it has been shown to provide cues that affect cell migration, proliferation, and differentiation [14]. ECM based scaffolds can even be of xenogeneic origin after successful decellularization to remove cellular antigens [44]. As a result, the xenogeneic ECM is used as a biological scaffold in tissue reconstruction and

transplantation. For example, the porcine ECM tissue resources are small intestine, porcine urinary bladder or porcine skin which are fabricated to biomaterial, such as Alloderm®. These scaffolds are giving the optimistic option in clinical treatment. Moreover, many ideas show whether the ECM scaffolds need to be seeded stem cells to do as a bioactive scaffold or only used as an decellular products [11]. Previous study reported that decellularized ECM was good for osteochondral repair applications [44].

Decellularized dental pulp ECM

In general, the ECM of dental pulp is similar with the ECM of other organs. It has many compositions which are proteins, glycoproteins, glycosaminoglycans, and small molecules. The compositions arrange in a unique of a three-dimensional architecture. Their distributions are different amount belong to different anatomic region. For example, amount of collagen type IV is represent within vascular membrane and epithelial tissue. Type III collagen is found within the submucosal tissue such as the urinary bladder [11]. The dental pulp is a loose connective tissue, characterized by its specific anatomical location [45]. Besides that, the ECM components of dental pulp distribute more special than soft connective tissues. The collagens is the highest components with many types, such as collagen type I, III, V, VI. The type I and type III collagens are the highest rate in dental pulp at 56 and 41%, respectively. The non-collagenous ECM components are represented in dental pulp, such as fibronectin, dermatan sulfate, and chondroitin 4- and 6-sulfate. Moreover, glycosaminoglycans (GAGs) are keratan sulfate, hyaluronic acid that are essential for wound healing process. Many growth factors components are also understood in dental pulp, such as bone morphogenetic proteins (BMPs), type IA and II receptors for transforming growth factor-beta (TGF-β) [17]. Other proteins also present in dental pulp as same as in bone such as bone sialoprotein, osteocalcin, osteopontin, and osteonectin [2, 17]. The above compositions are necessary to fabricate a scaffold in bone tissue engineering. In previous study, Traphagen *et al.* reported the collagenase method properly to decellularize porcine tooth bud. After decellularization, the collagen I, collagen IV, fibronectin, and laminin were detected in

decellularized specimens [46]. In previous study, the decellularized dental pulp combine with silk and collagen may potential ECM scaffold for bone tissue engineering [18]. The decellularized dental pulp which coated on silk fibroin scaffold improved the cell biofunctionalities. The silk fibroin scaffolds coated with decellularized dental pulp kept the 3D structure and enhanced much fibrils among their interconnective pores that encouraged bone cells adhesion, growth, and differentiation [47].

Chapter 2

Objective

General Objective

To evaluate the silk fibroin scaffolds coated with fibronectin and decellularized dental pulp (SF-FP) generating new bone formation in the rabbits' calvarial defects.

Specific Objectives

1. To evaluate the compatibility of the SF-FP scaffolds.
2. To assess the amount of the new bone formation was enhanced by SF-FP scaffolds.
3. To compare the new bone formation among the SF-FP scaffolds, silk fibroin scaffolds, and autogenous bone graft *in vivo* experiment.

Benefit of the study

Providing the specific knowledge of the silk fibroin scaffolds coated with fibronectin and decellularized dental pulp to enhance new bone formation.

Hypothesis

The silk fibroin scaffolds coated with fibronectin and decellularized dental pulp could be biocompatible and could enhance new bone formation in the rabbits' calvarial defects.

Chapter 3

Materials and Methods

Materials

Coating Silk Fibroin Scaffolds

Silk fibroin scaffolds preparation

The three-dimension (3D) *Bombyx mori* silk fibroin scaffolds were prepared by following steps. First, boiling the *Bombyx mori* fiber cocoons for 30 minutes in 0.02 M Na_2CO_3, then rinsed with a distilled water 3 times for 20 minutes/ time to extract sericin. Second, the silk fibers were dried in hot air oven at 60^0C for 24h. Third, the silk was dissolved in 9.3 M LiBr solution at yielding the 3% (w/v) silk fibroin solution and incubated at 60^0C for 4h [48]. Then silk fibroin solution was centrifuged for 20 min at 9000 rpm (4^0C) [49]. Finally, the silk solution was purified by dialyzing against distill water for 3 days. The silk fibroin solution will be stored at 4^0C until further using [32, 50]. After extraction sericin protein, the 3D porous silk fibroin scaffolds were fabricated through following lyophilization method. Firstly, the silk fibroin solution was prepared in 48 well plates. Secondly, they were generated porous by freeze- drying machine in 30 minutes. Then, each silk scaffold was treated by immersing in 70% (w/v) methanol for 30 minutes. After that, the porous silk scaffolds were freeze-drying again 30 minutes [50]. Finally, all scaffolds will be prepared in 10 mm in diameter and 2 mm in thickness.

Fibronectin

The fibronectin solution was prepared from a fibronectin powder as following procedure. The commercial fibronectin powder was the bovine plasma (Fibronectin from Bovine plasma, cat. # F4759, Sigma Aldrich) which passed a cell attachment assay and cell toxicity assay of the commercial company. It dissolved in sterilized water by 1mg: 1ml ratio at 37^0C for 30 minutes. The solution was stored in a refrigerator until further using.

Decellularization of teeth pulp tissue

The research was approved by Research Ethics Committee, Faculty of Dentistry, Prince of Songkla University (MOE 0521.1.03/486). The primary teeth which were indicated for extraction were collected from the patients. Inclusion criteria: all primary teeth of the 6-12-year-old children were indicated for extraction, such as orthodontic reasons, prolong retention of primary teeth. Exclusion teeth: Decay teeth, injured teeth, odontogenic infections teeth, or children have systemic diseases. The teeth were put in a Dulbecco modified Eagle's Media (DMEM) (Biowhittaker, GIBCO, Sigma, USA) with a Penicillin/ Streptomycin (Invitrogen Co., USA) and a 10% fetal bovine serum (FBS) (JRH Biosciences, Inc., Lenexa, KS, USA). The teeth were cut in half collecting the dental pulp tissue by a sterile dental probe. The dental pulp tissue was kept in the DMEM, then was digested by a collagenase type I (3mg/ml) (Sigma, USA) for 60 minutes at 37^0C in an incubator. The decellularized dental pulp and cells were separated by a mesh (Falcon® 100µm Cell Strainer, Corning, USA). Collecting decellularized dental pulp from mesh and keeping at -80^0C for 24h.

Preparation of coated silk scaffold

The 3D silk fibroin scaffolds were cut into disc (10-mm in diameter and 2-mm in thickness), then were sterilized in a 70% ethanol, and soak in a PBS for overnight. Then, the fibronectin and the decellularized dental pulp tissue were prepared, with 1:1 ratio, as sterile aqueous solution. The silk scaffold independently incubated with the 0.1mg/ml coating solution for 1h at 37^0C, following to dry in a laminar flow hood for 1h at room temperature.

Observation Scaffolds' Surfaces by SEM

Scanning Electron Morphology (SEM) was used to observe the SF-FP and SF scaffolds' surfaces. A scaffold of each group was chosen randomly for observing and evaluated morphometry and characteristic of coating, such as pore size, porosity of the scaffolds. In SEM preparation, the scaffolds were coated with gold by a gold sputter- coating machine (SPI supplies, Division of Structure Probe Inc., Westchester, PA, USA). Then the scaffolds were observed their morphometry and

characteristic by a SEM (Quanta 400, EI, Czech Republic). The pore size and porosity of the SF and SF-FP scaffolds were analyzed by ImageJ software (Wayne Rasband) developed at the US National Institutes of Health.

In vivo experiment

Animal models

Eighteen male New Zealand white rabbits were 2.5- 3 kg (2.70 ±0.22 kg) to use in the present study [51, 52] (**Fig. 1**). The caring protocol of the animals were performed as the standard animal care protocol of the Faculty of Science (MOE 0521.11/520).

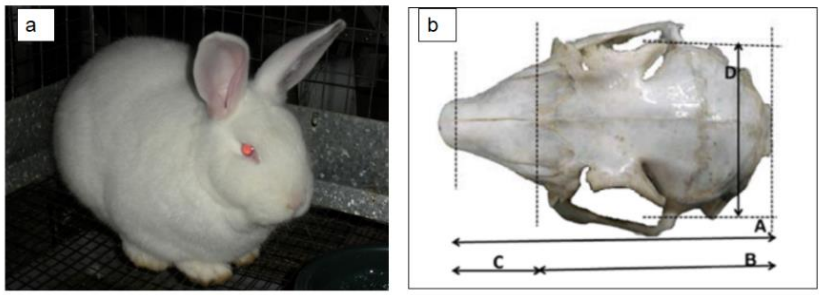

Fig. 1 The rabbit experimental model (a) New Zealand white rabbit; (b) The rabbit's skull. A: Skull length 91mm, B: Cranial length 61mm, C: Nasal length 33mm, D: Cranial width 31mm.

Methods

Group of Study

The eighteen rabbits were randomly divided into three groups that received the following implants: group 1, the silk fibroin scaffold (SF) (n=6); group 2, the silk fibroin scaffold coated with fibronectin and decellularized dental pulp (SF-FP) (n=6); and group 3, the cortical autogenous bone chip (AB) (n=6). The defects were created both sides of the parietal calvarial bone. The distribution of the experimental groups was in **Table 1**.

Table 1 The distribution of the experimental groups

Groups	Description	Animal	Defects
1	Silk fibroin scaffold (SF)	6	12
2	Silk fibroin scaffold coated with fibronectin and decellularized dental pulp (SF-FP)	6	12
3	Autogenous bone (AB)	6	12
Total		**18**	**36**

Experiments

Anesthetic Phase

All rabbits were placed on the surgical table in prone position. Anesthesia was induced by the 25mg/kg ketamine hydrochloride and 5 mg/kg diazepam intramuscularly into the gluteal muscle region. Three minutes later, an intravenous catheter was placed in the marginal ear vein for intravenous anesthesia (**Fig. 2**). After that, the 5 mg/kg thiopental was administered intravenously and was titrated at the rate of 2mg/kg every 15 minutes (maximum dose is not more than 30 mg/kg) until achieving unconsciousness. Additionally, the penicillin G solution (50,000U/kg) was given for prophylaxis.

Fig. 2 The anesthesia intravenous injection at the marginal ear vein

Operative Phase

All surgical procedures were performed under aseptic conditions by the same surgical team. The surgical field was shaved and was disinfected with a 10% povidone- iodine over the cranium area between both ears of the rabbit. Then local

anesthesia injection was made at the skin area of the surgical field by vasoconstrictor (1.8 ml of 2% lidocain hydrochloride with 1:100,000 epinephrine).

After that, a 3-cm mid sagittal incision was made on surgical area. Subperiosteal dissection was carried out. A sterilized 10-mm circular aluminum template was used to ensure the same critical-size defects in each side of each rabbit. The bilateral bicortical bone defects of the 10-mm circular diameter were created at the left and right parietal bone carefully. Each defect was made approximately 1 mm far from the sagittal suture. The 0.9% NaCl solution was used to irrigate, to clean out abraded particles, to reduce the hot temperature from drilling, and to avoid bone necrosis. The four 1-mm holes were drilled around the defects by a round bur and filled with pre-heated gutta-percha. These holes was used to identify the defects for evaluating later (**Fig. 3**).

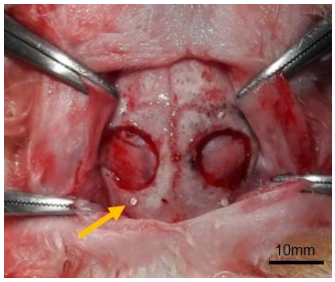

Fig. 3 The 1-mm holes were filled by gutta-percha (yellow arrow)

At the group 1, 2, the SF-FP and SF scaffolds were soaked in the 0.9% NaCl for 10 minutes. In group 3, autogenous bone particles that was collected from the procedure was minced by a bone morselizer (Salvin Dental Specialties Inc., Charlotte, NC, USA). The amount of the autogenous bone was calibrated to have the equal volume with the scaffold using an acrylic mold and were further weigh (**Fig. 4**).

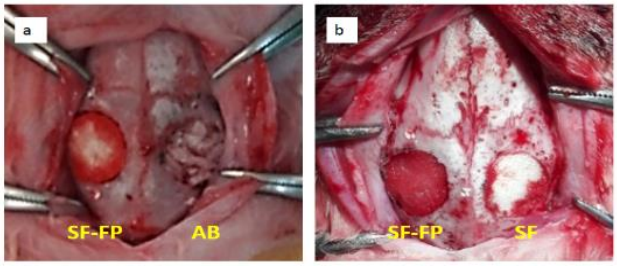

Fig. 4 The experimental materials filled the calvarial defects (a) SF-FP and AB; (b) SF-FP and SF.

These grafting materials were chosen to implant randomly Table **2**) The wound was closed in layer-by-layer with Viryl® 4.0 suture.

Table 2 The random sides of the experimental materials. R: right side, L: left side.

Number of Rabbits	**Test sides**	**Materials**	**Specimen labels**
1	1R	SF-FP	1A
	1L	SF	1B
2	2R	SF-FP	2A
	2L	AB	2C
3	3R	SF	3B
	3L	AB	3C
4	4R	SF-FP	4A
	4L	SF	4B
5	5R	SF-FP	5A
	5L	AB	5C
6	6R	SF	6B
	6L	AB	6C
7	7R	SF-FP	7A
	7L	SF	7B
8	8R	SF-FP	8A
	8L	AB	8C
9	9R	SF	9B
	9L	AB	9C
10	10R	SF-FP	10A
	10L	SF	10B

Table 2 The random sides of the experimental materials. R: right side, L: left side. (Cont.)

Number of Rabbits	Test sides	Materials	Specimen labels
11	11R	SF-FP	11A
	11L	AB	11C
12	12R	SF	12B
	12L	AB	12C
13	13R	SF-FP	13A
	13L	SF	13B
14	14R	SF-FP	14A
	14L	AB	14C
15	15R	SF	15B
	15L	AB	15C
16	16R	SF-FP	16A
	16L	SF	16B
17	17R	SF-FP	17A
	17L	AB	17C
18	18R	SF	18B
	18L	AB	18C

Postoperative Phase

Each rabbit was in a single cage, looked out a standard pellet and water ad libitum. They were monitored for recovery carefully. The single dose of the pethidine (10mg/kg) was administered intramuscularly for analgesic. As antibiotic therapy, the PGS (50,000- 100,000 U/kg) was injected intramuscularly once daily for three days and the wound was dressed once a day during the three days post- operative period. Thereafter, the clinical changes of the rabbits were closely followed up and recorded, such as swelling, color, inflammation, and tissue necrosis.

Sacrifice Period

The experimental animals were sacrificed at 2, 4, 8 weeks postoperative time points by an overdose pentobarbital sodium 200mg/ml intravenously (**Table 3**). Then the rabbits' calvaria were removed in the one-block specimens. They were put in

a 10% formalin immediately for a week before being evaluated by radiography, micro-computerized tomography (micro-CT), and histology.

Table 3. The sacrifice postoperative time points

Time point	Number of defects			Total
	SF	SF-FP	AB	
2 weeks	4	4	4	12
4 weeks	4	4	4	12
8 weeks	4	4	4	12
Total	12	12	12	36

Evaluation

Radiography Evaluation

The radiographs of the specimens were obtained at 2, 4, 8 weeks postoperative time points. All digital radiographs were taken by a hand-held portable X-ray device (NOMAD, Aribex Inc., Utah, USA), setting exposure 60 Kvp, 3 mA, at 0.10 sec, using the digital sensor size 1 (SOPIX^2 sensor, Aceton Inc., France) attaching to digital sensor holder (XCP-DS, Rinn, Densply, IL, USA) to control the 15-cm vertical distance. The radiographs were recorded in an imaging software (Sopro Imaging 1.71, Aceton Inc., France) (**Fig. 5**). Then, the mean of optical density (Mean OD) of the defects were calculated and analyzed by software Image Pro Plus version 7.0 (Media Cybernetics; Silver Spring, MD, USA) with a intensity calibration 0 - 255 ratio gray scale as default. The Mean OD was counted pixels within the object per area of each defect. They were measured three times to minimize an error and compared an amount mineralization of the experimental materials.

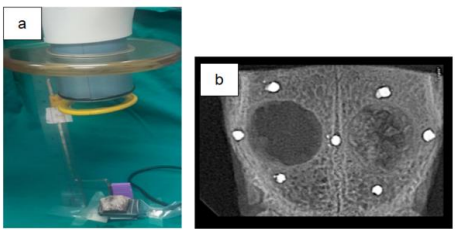

Fig. 5 Radiography examination. (a) The digital radiography procedure; (b) a recorded radiograph of the one-block specimen.

Micro-computerized Tomography (micro-CT)

A high resolution micro-CT system (Micro-CT35, Scanco, Medica AG, Bassersdorf, Switzerland) was used (**Fig. 6**). Each specimen was put in a vertical position in a 15ml 10% formalin sample holder to keep sample in a same contrast, and to avoid a damage due to scanning period. The specimens were scanned perpendicularly at 70 kVp, 113 µA, and 8 W in high- resolution mode (18.5 μm^3/ voxel). The volume of interest (VOI) was defined by the gutta-percha markers of the specimens; they pointed to scan the contour region of the interest area.

In an imaging process, a Gaussian filter standard deviation was 0.8- 2 to decrease the noise. A gray scale threshold value was determined to discriminate the original bone, the new bone formation. The scanned data were reconstructed by a built-in software (µCT Tomography V6 1-2, Scanco, Media AG, Bassersdorf, Switzerland). This allowed the creation of the three dimension (3D) reconstructive images of the defects. The region of interest was analyzed using the following parameters, bone volume fraction (BVF): percentage of bone volume by total defect volume (percentage of BV/TV), trabecular thickness (mm) and bone mineral content (mgHA/ccm).

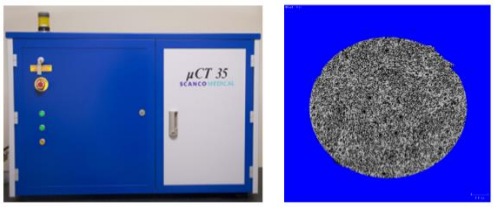

Fig. 6 Micro-CT35 scanner and 3D- reconstruction of the half of calvarial specimen.

Histological Evaluation

The calvarial specimens were decalcified in a 10% formic acid which was subsequently changed every day for three weeks. The specimens were decalcified by a 10% EDTA, adjusted pH 7.4. Then they were cut into two pieces, each piece had an experimental scaffold or bone graft material. Both pieces were trimmed until they encroached on the grafting area. They were divided into two pieces at the midline before dehydrating in graded series of alcohol with an automatic tissue processor (Leica TP 1020) and embedded in paraffin blocks. Each specimen was sectioned along

a sagittal plane by a diamond saw microtome, they were in 5-µm thickness of three serial sections of each specimen (**Fig. 7**). Each histological section was stained by a haematoxylin and eosin (H&E) in one mounted glass slide. In summary, three slides from the center of each experimental material were represented for each defect and examined under a light microscope to observe the newly formed bone, inflammatory cells response, vascula.

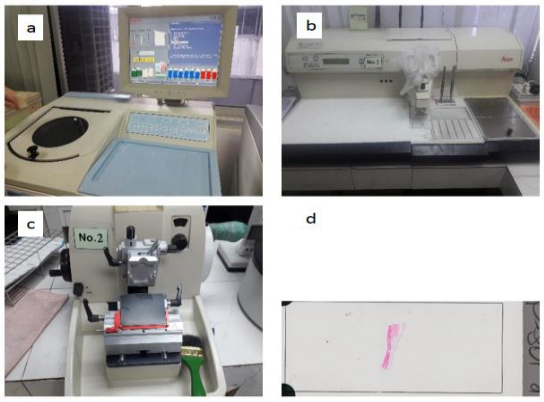

Fig. 7 The histological preparation. (a) The automatic dehydration process, (b) Paraffin embedding station, (c) Rotary microtome for cutting specimens, (d) Slide of specimen with H&E staining.

Statistical analysis

A descriptive study was used to evaluate the material, clinical, radiography examination and histological observing aspects. The total bony defect area, area of new bone formation and percentage of bone area was measures three times separately to minimize bias. The numerical data were presented in Mean ± Standard Deviation (SD). Using Kruskal- Wallis test, following by Mann-Whitney U test to find out the difference among three experimental groups in each study period (2, 4, 8 weeks). P-value less than 0.05 considered statistically significant difference. All the data were subjected to SPSS (Statistical Package for the Social Sciences, IBM, USA) version 16.0.

Chapter 4

Results

Coated Silk Fibroin Scaffolds

All 3D porous structures of the SF and SF-FP scaffold were fabricated at 10 mm in diameter and 2 mm in thickness (**Fig. 8**). The SF-FP and SF scaffolds were dry, soft and much porosity.

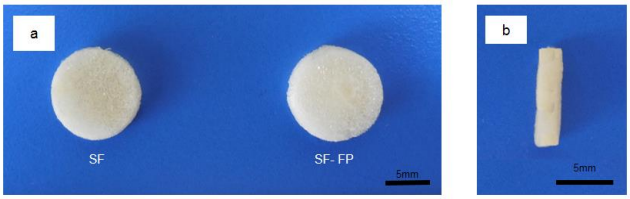

Fig. 8 The 3D porous scaffolds were prepared for in vivo experiment. (a) The scaffolds were at 10mm in diameter of the SF and SF-FP scaffolds; (b) The SF-FP scaffold was at 2 mm in thickness.

SEM observation

The morphologic surfaces of the SF and SF-FP scaffolds were scanned by SEM at magnification of 50x and 500x. The SF scaffold was thin boundary, and high interconnective porosity. The SF-FP scaffold was thicker boundary, high interconnective porosity, and increased fibrils and particles on the walls (**Fig. 9**).

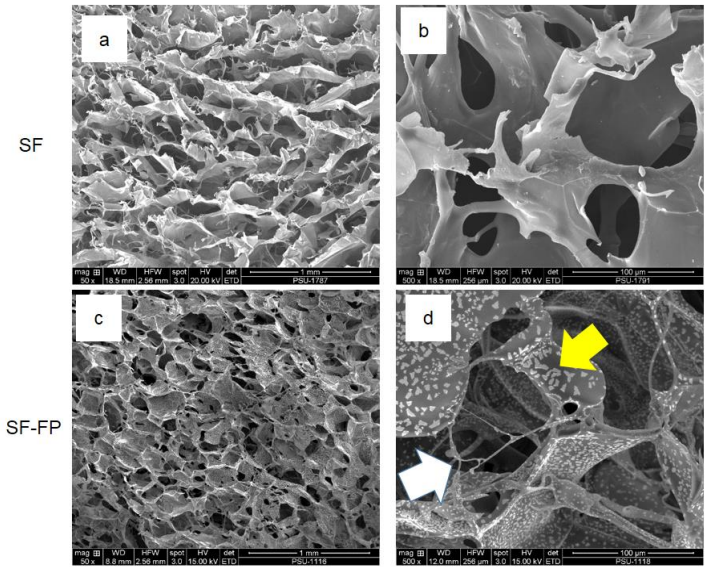

Fig. 9 The morphologic surfaces of the scaffolds were scanned by SEM. The morphologic surface of the SF scaffold, (a) at 50x, the SF scaffold was large pore diameter, thin walls and high interconnective porosity; (b) at 500x, the SF scaffold was smooth and thin boundary. The morphologic surface of the SF scaffold, (c) at 50x, the SF-FP scaffold was smaller pore diameter, thicker boundary, and high interconnective porosity; (d) at 500x, the SF-FP scaffold presented fibril structure at inner pores (white arrow), and decellularized dental pulp attached on the walls (yellow arrow).

The porous features of the SF and SF-FP scaffolds were analyzed by ImageJ in **Table 4**. The pore size of the SF-FP was significantly smaller than the SF's ($p<0.001$). Their porosity was quite similar at 85.32% of the SF scaffold, and 83.395% of the SF-FP scaffold

.

Table 4 The porous features of the experimental scaffolds. The value of porous size in micrometer (μm) was showed by Mean ± SD, and the percentage of porosity (%). a = statistically significant difference ($p<0.001$).

	Porous size	**% Porosity**
SF	162.0114 ± 10.01 μm	85.32 %
SF-FP	109.3659 ± 10.21 μm [a]	83.39 %

Clinical Evaluation

All animals were treated well due to anesthesia and surgical procedure. After they were full recovery from surgery, they ate and drank water ad libitum. All rabbits lived throughout the experiment. All wounds healed excellent without any evidence of infection or wound dehiscence. In the sacrifice time points, the pericranium exposure healed without any infection. They were intact the layers of underlying brain and dura (**Fig. 10**).

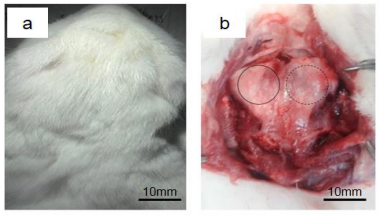

Fig. 10 The healing of the rabbit calvarium at 8 weeks postoperative (a) Growth of normal hair, no infection, no wound healing dehiscence; (b) Complete healing at pericranium. Solid circle= the SF-FP scaffold; Dash circle = the SF scaffold.

Gross Specimen Observation

The 18 rabbits were sacrificed at 2, 4, 8 weeks postoperative time points. The calvaria were harvested in the one-block specimens. At the 2 weeks postoperatively, the SF and SF-FP groups were smooth, covering well without any fistula and infection evidence at both pericranium and endocranium sides (Fig. 11). They decreased a few of the critical-size defects. Both of the experimental groups

swelled. The color of them was better pink than peripheral area. Both of two scaffolds were rubbery at the middle when palpation. In the other hand, the AB group healed better than the experimental groups without any infection and firm.

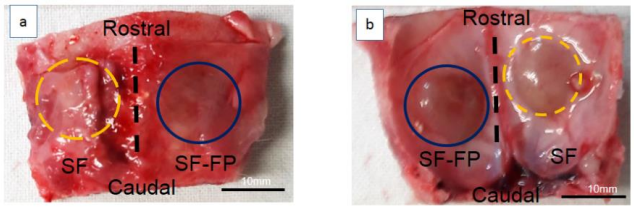

Fig. 11 The SF and SF-FP block gross specimen at 2 weeks. (a) The pericranium was good healing over the scaffolds' surfaces. (b) The endocranium membrane covered well at the scaffolds' sites, the endocranium membrane swelled. A spot at SF side was from the gutta-percha marker.

At 4 weeks postoperative time point, the SF and SF-FP groups were smooth and covered well, but also not any infection as pus or fistula at both pericranium and endocranium sides (**Fig. 12**). They decreased their size defects more than 2 weeks. They did not swell. The periphery of the SF-FP and SF groups were firm. The SF-FP and SF groups were rubbery consistency at the middle. In the other hand, the AB group was better healing without any swelling or infection, similar color, and firm consistency.

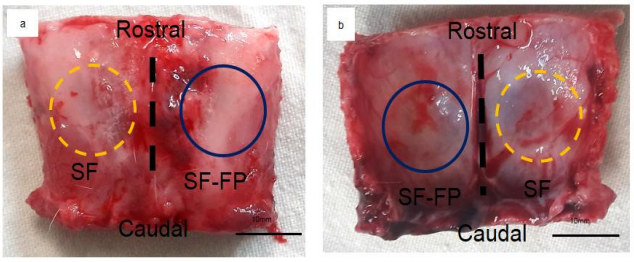

Fig. 12 The specimen of the calvarial rabbit at 4 weeks. (a) The periosteum was good healing over scaffolds surface. (b) The endocranium membrane covered well at the scaffolds' sites.

At 8 weeks postoperative time point, the SF and SF-FP groups were smooth and covered well. They decreased their critical-size defects, similar color with host tissue. They were firm at periphery and rubbery consistency at their middle (**Fig. 13**). In the other hand, the AB group was better healing without any swelling or infection, similar color. It was rubbery consistency as same as host bone.

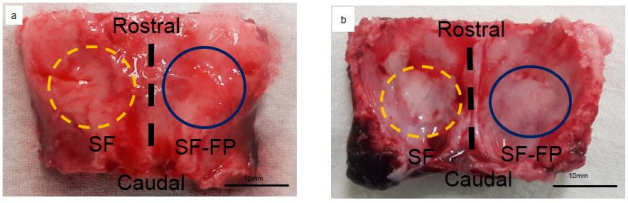

Fig. 13 The specimen of the calvarial rabbit at 8 weeks. (a) The pericranium was good healing over scaffolds surface. (b) The endocranium membrane covered well at scaffolds sites, similar color as host bone. They were firm consistency at periphery and rubbery consistency at middle.

Radiography Evaluation

All specimens were taken the radiographs to evaluate the density of the new bone formation in the defects (**Fig. 14**). At the SF group, the radiopaque increased gradually at the defects' periphery throughout the experimental period. At the SF-FP group, the radiopaque area increased gradually at the defects' periphery at 2, 4 weeks, especially at 8 weeks, the radiopaque developed and moved into the center of defects. In AB group, it was high radiopaque in defects at 2weeks, and absorbed gradually as same as bone outside defect at 4 weeks, 8 weeks at 50%, and 100%, respectively.

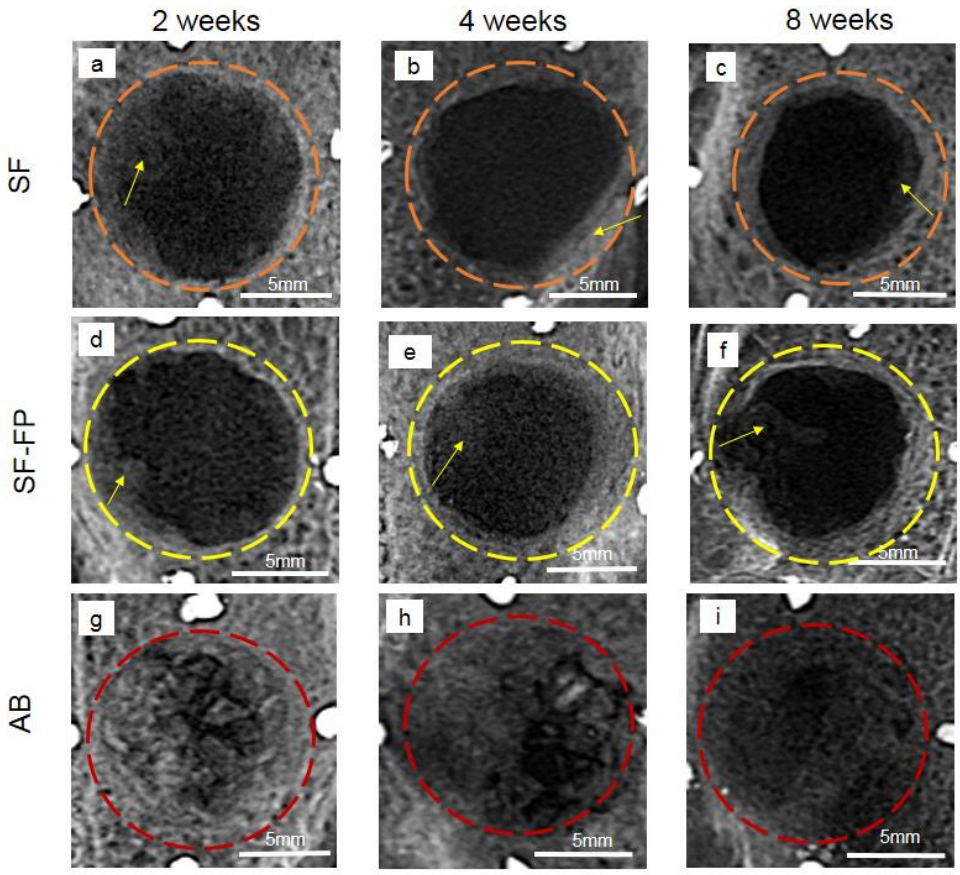

Fig. 14 The radiographs of the rabbit calvaria defects. (a, b, c) At the SF group, the radiopaque increases gradually at the periphery at 2, 4, 8 weeks. (d, e) At the SF-FP group, the radiopaque increased gradually at periphery at 2 and 4 weeks, (f) especially at 8 weeks, the radiopaque moved to the center of the defect. (g, h, i) In AB group, bone graft were absorbed gradually as same as bone outside defect from 2 weeks, 50% at 4 weeks, and 100% 8 weeks. *Yellow arrow*= radiopaque area of the defect.

The mean optical density results were in **Table 5**. The SF group increased 2% from 2-week to 4-week postoperative. Nevertheless, it decreased approximately 12% at 8-week postoperative. The SF-FP and AB groups were higher than SF groups at 2-, 4-, and 8-week postoperatively. The SF-FP and AB groups' OD decreased gradually. They showed statistically significant different among the AB, SF, and SF-FP groups *($p<0.05$)*.

Table 5 The OD results of the experimental groups. The value was pixel, mean ± SD.
a = statistically significant difference ($p<0.05$)

	2 weeks	**4 weeks**	**8 weeks**
SF	47.536 ± 8.568	50.444 ± 5.028	38.752 ± 8.131
SF-FP	56.9 ± 6.419	53.354 ± 9.975	43.416 ± 2.246
AB	75.35 ± 12.61 [a]	70.863 ± 5.882 [a]	67.610 ± 14.027 [a]

Micro-CT Examination

All the specimens were reconstructed in the 3D images (**Fig. 15**). The SF implants enhanced new bone formation at the periphery. The SF-FP implants enhanced the new bone formation at the periphery at 2 and 4 weeks. Then, the bone density enhanced forward into the center of the defect at 8 weeks postoperatively. The defects of the AB group were healed gradually at 2 weeks, 4 weeks, and filled completely at 8-week postoperative.

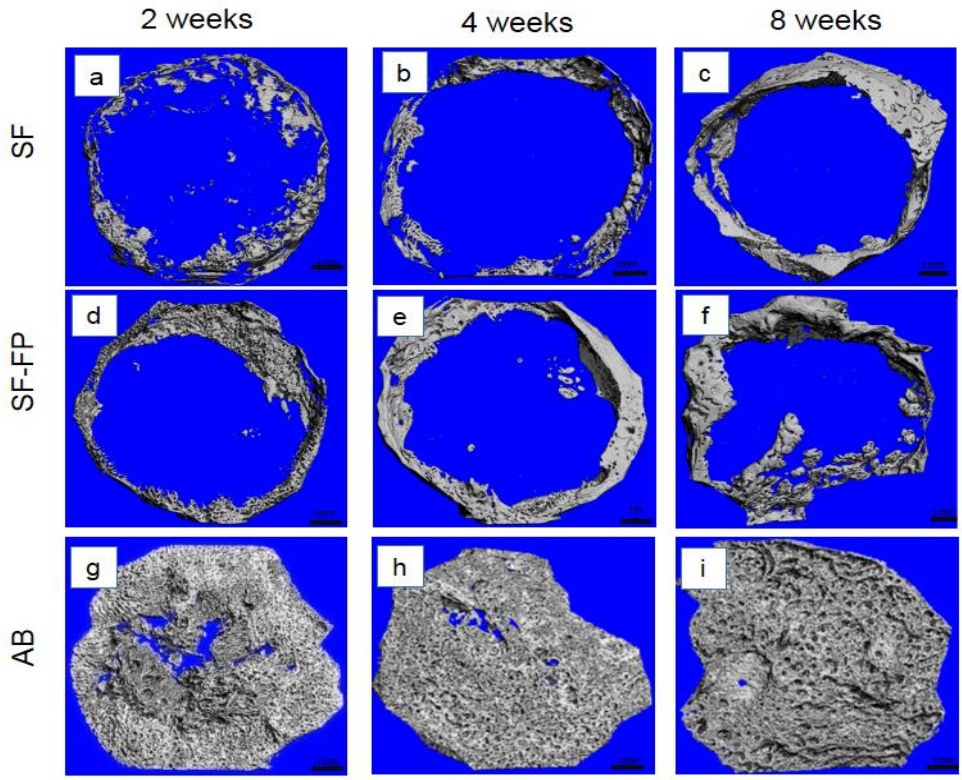

Fig. 15 The 3D reconstructive images of the experimental groups at 2 weeks, 4 weeks, and 8 weeks postoperative time points. The SF implants enhanced new bone at peripheral area of the defects (a, b, c). The SF-FP implants enhanced new bone formation and were better density than the SF implants at the periphery at 2 weeks (d), 4 weeks (e); then the new bone formation moved forward into the center of the defect at 8 weeks (f); and the defects of the AB group increased the bone formation gradually at 2 weeks (g),4 weeks (h), and healed completely at 8 weeks (i).

MicroCT analysis

In **Table 6**, the new bone percentage of AB group was highest and increased gradually from 2 weeks to 8 weeks. The second place was the SF-FP group, and the lowest was the SF group. The SF and SF-FP groups increased from 2 weeks to 4 weeks approximately 1.3% and 2.6%, respectively. However, at 8 weeks they decreased about 0.5% and 2 %, respectively. The new bone percentage of the SF-FP group was higher than the SF group's in all postoperative time points. There were significant different among the AB group and the experimental groups in postoperative time points ($p<0.05$).

Table 6 The percentage of the bone volume fraction (% BV/TV). The value was in mean± SD (%). a = statistically significant difference ($p<0.05$).

	2 weeks	**4 weeks**	**8 weeks**
SF	4.34 ± 2.79	5.60 ± 3.40	5.23 ± 2.52
SF-FP	6.89 ± 1.45	9.52 ± 1.42	7.66 ± 3.07
AB	30.24 ± 7.00 [a]	32.74 ± 7.33 [a]	33.82 ± 5.81 [a]

Table 7 summarized the trabecular thickness of the experimental group in all postoperative time points. The trabecular structure of the AB group was the highest among three groups, following by the SF-FP group, and the lowest was the SF group. The results of the SF and SF-FP group increased at 4 weeks, and slightly decreased at 8 weeks. There was significant different between SF-FP group and SF group at 4-week ($p<0.05$). There was not significant different at 2 weeks, but was

significant different among the AB, SF, SF- FP groups at 4 weeks, and 8 weeks ($p<0.05$).

Table 7 The results of the trabecular thickness in micrometer (mm). The value was mean± SD. a= statistically significant difference among groups ($p<0.05$), b= statistically significant different between the SF group and SF-FP group.

	2 weeks	**4 weeks**	**8 weeks**
SF	0.117 ± 0.0477	0.1272 ± 0.0254	0.1125 ± 0.056
SF-FP	0.1638 ± 0.046	0.176.3 ± 0.0183 [b]	0.1482 ± 0.0227
AB	0.1981± 0.0153	0.2048 ± 0.0178 [a]	0.1931± 0.0151 [a]

Table 8 showed the bone mineral density of three groups in all postoperative time points. The AB group was the highest; it increased gradually due to postoperative time points. The trend of the SF and SF-FP groups increased from 2 weeks to 4 weeks, and decreased at 8 weeks. The bone mineral density of the SF-FP group was higher than the SF group in all time points. There was significant different among the AB, SF-FP, SF groups ($p<0.05$).

Table 8 The bone mineral density of the experiments in all three time points. The value was mean± SD, and measured by mgHA/ccm. a= statistically significant difference ($p<0.001$).

	2 weeks	**4 weeks**	**8 weeks**
SF	59.2186±16.5271	64.6619±29.4761	54.0948±18.2125
SF-FP	92.5712±18.9865	96.6212±20.1680	65.3746±21.2883
AB	305.91±54.7358 [a]	310.81±57.2127 [a]	311.45±46.2386 [a]

Histology evaluation

The 36 specimens were cut in the 5-μm section series and stained with H&E to evaluate in histology. The new bone growth, blood vessels and inflammatory cells were observed in the slides of three experimental groups.

The histology of the AB group was at 2 weeks (**Fig. 16**). The new bone formation enhanced among the defect with light color at the periphery of the AB and host bone (**Fig. 16a**). The new bone formation was light pink color, irregular shapes from the host bone and bone grafting material either at the periphery (**Fig. 16b**) and the middle of the defect (Fig. 16**c**). The blood vessels were much between the new bone and grafting material. There did not represent the inflammatory cells among the defect. The **Fig. 17** showed the SF defect at 2 weeks. The SF scaffold swelled, the homogenous purple color was at the filled defect (**Fig. 17a**). The new bone formation represented at the periphery (**Fig. 17b**). Further, the center showed much foreign-body giant cells, inflammatory cells, rare vessel within the residual SF scaffold (**Fig. 17c**). The SF-FP group's histology was at 2 weeks (Fig. 18). The shape of the SF-FP implant did not swell, and the color was pink and less dark purple as the SF group's (**Fig. 18a**). The new bone formation was detected at the periphery, and was irregular (**Fig. 18b**). The middle of the SF-FP scaffold could not detect new bone formation, but it was much blood vessels, less giant cells and inflammatory cells (**Fig. 18c**).

At 4 weeks, the AB group showed good healing at the defect (**Fig. 19a**). The new bone formation grew regular nearly, and was not homogenous color, the bone marrow also presented inside bone. It was very difficult to detect the periphery (**Fig. 19b**). As same as at the middle site, the new bone formation and bone marrow grew up within the defect, could not detect the residual bone graft material (**Fig. 19c**). At 4 weeks, the overall shape of the SF implant was slightly collapse. The color turned pinker than it is at 2 weeks (**Fig. 20a**). The new bone formation was detected at the periphery, it did not enhance further than the periphery (**Fig. 20b**). Moreover, the giant cells and inflammatory cells were much. The vascularization enhanced few. The residual scaffold was detected at the middle of the defect (**Fig. 20c**). The SF-FP group's histology was at **Fig. 21**. It kept the thickness size, and the color looked like inflammatory reaction (**Fig. 21a**). The new bone formation was at the periphery. The residual scaffold presented among the new bone formation. The new bone formation enhanced further than the periphery (**Fig. 21b**). However, the new bone formation was not detected at the middle site. At the middle, the blood vessels

was induced more than the SF group. The foreign-body giant cells and inflammatory cells were few. The residual scaffold was detected at the middle of the defect (**Fig. 21c**).

At 8 weeks, the AB implant was showed homogenous pink color between the defect and host bone. It slightly collapsed rather than at 4 weeks (**Fig. 22a**). It was difficult to detect the gap of bone graft and host bone at the periphery. It was less the new bone formation and the bone arranged as the mature bone. The fatty bone marrow was detected among the bone formation (**Fig. 22b, c**). At the same 8 weeks postoperative, the SF scaffold collapsed, it did not keep the normal size (**Fig. 23a**). The new bone formation still inhomogeneous, there was residual material inside the new bone formation at the periphery (**Fig. 23b**). At the middle, all were fibrous tissue, a few of the residual scaffold was detected (**Fig. 23c**). The SF-FP implant collapsed as same as the pattern of the SF implant at 8 weeks postoperatively (**Fig. 24a**). However, the new bone formation was enhance more than the SF group's at the periphery. It was more mature and enhanced further than the periphery (**Fig. 24b**). The fibrous tissue induced much, and few of the residual scaffold or inflammatory cells were detected at the middle site (**Fig. 24c**).

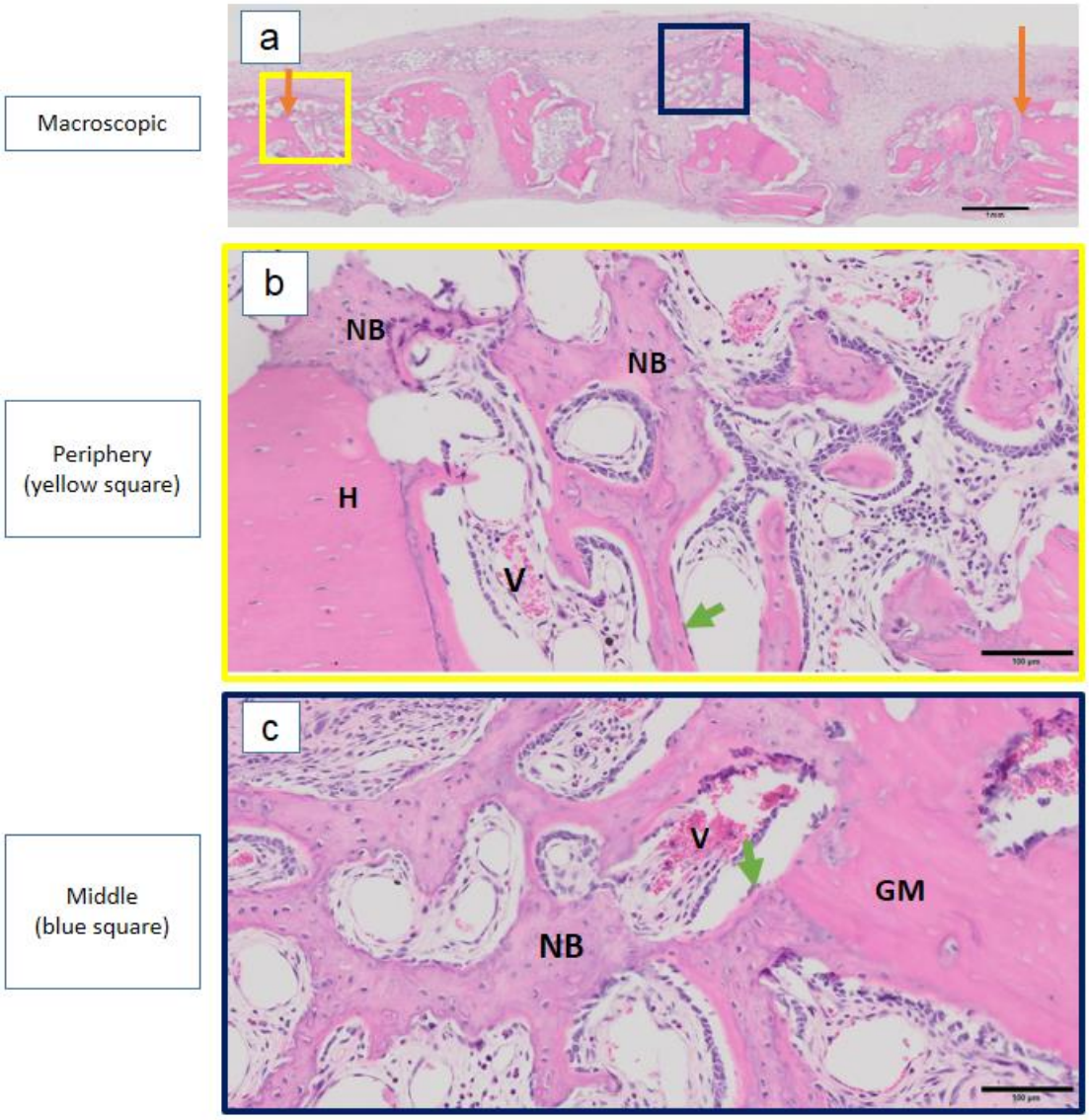

Fig. 16 The histology of the AB group at 2 weeks. (a) The light pink of the new bone formation at the defect, scale bar: 1mm. The periphery site (yellow square) was focused at (b). The middle site (blue square) was focused at (c). Scale bars: 100µm. H: Host bone, NB: new bone, V: vascula, GM: residual graft material, Orange arrow: the margin of the defect and host bone, Green arrow: osteoblast.

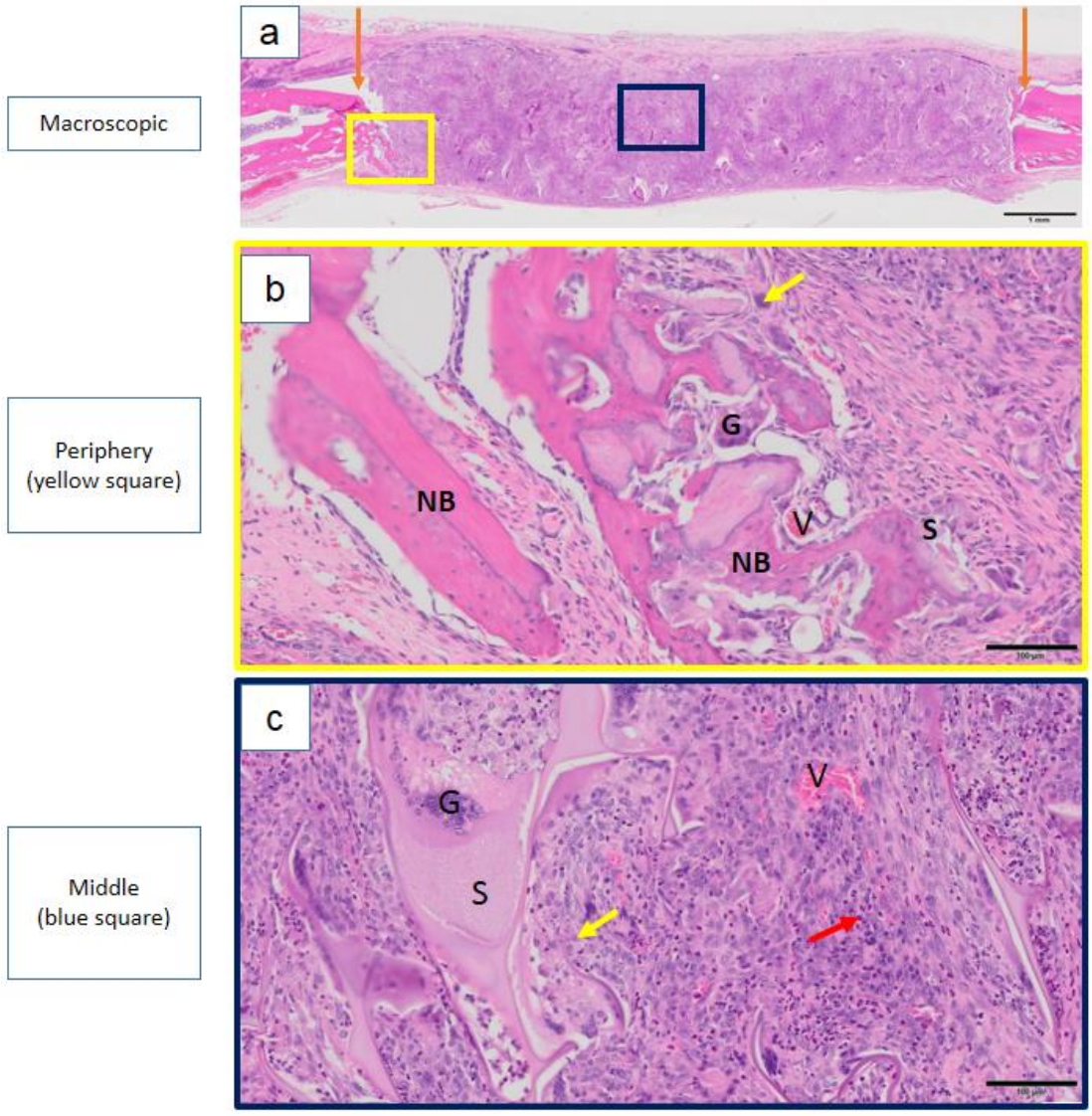

Fig. 17 The histology of the SF scaffold at 2 weeks. (a) The SF implant swelled and was filled by homogenous purple color of the inflammatory cells, scale bar= 1mm. The periphery (yellow square) was focused at (b). The middle site (blue square) was focused at (c). Scale bars: 100μm. H: host bone, NB: new bone, V: vascula, S: residual silk material, G: foreign-body giant cells, Orange arrow: the margin of the defect and host bone, Yellow arrow: macrophage, Red arrow: inflammatory cells.

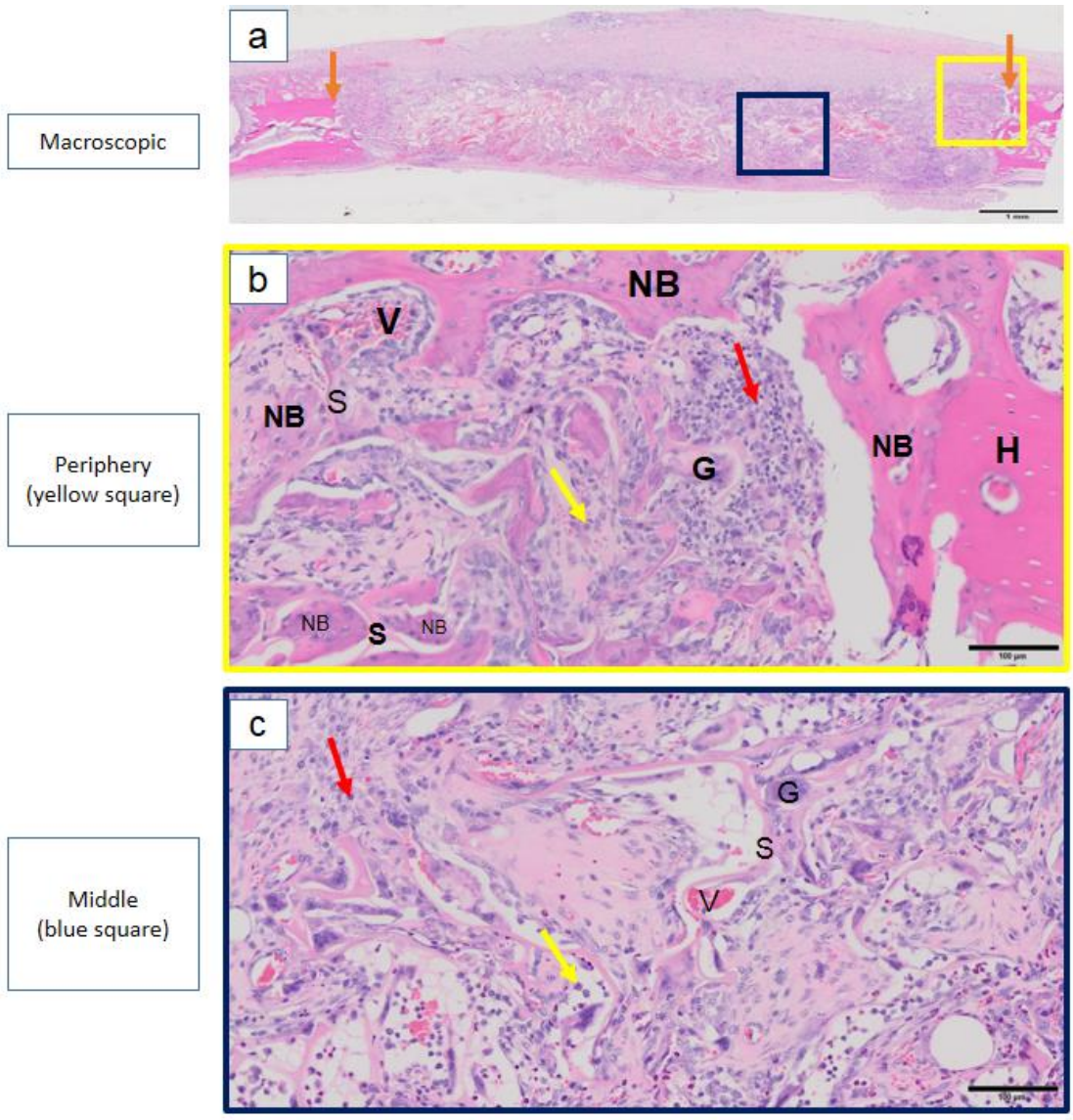

Fig. 18 The histology of the SF-FP group at 2 weeks. (a) The pink color of the vascularization and the purple color of the inflammatory cells presented within the defect, scale bar= 1mm. The periphery (yellow square) was focused at (b). The middle site (blue square) was focused at (c). Scale bars: 100μm. H: host bone, NB: new bone, V: vascula, S: residual silk material, G: foreign-body giant cells, Orange arrow: the margin of the defect and host bone, Yellow arrow: macrophage, Red arrow: inflammatory cells.

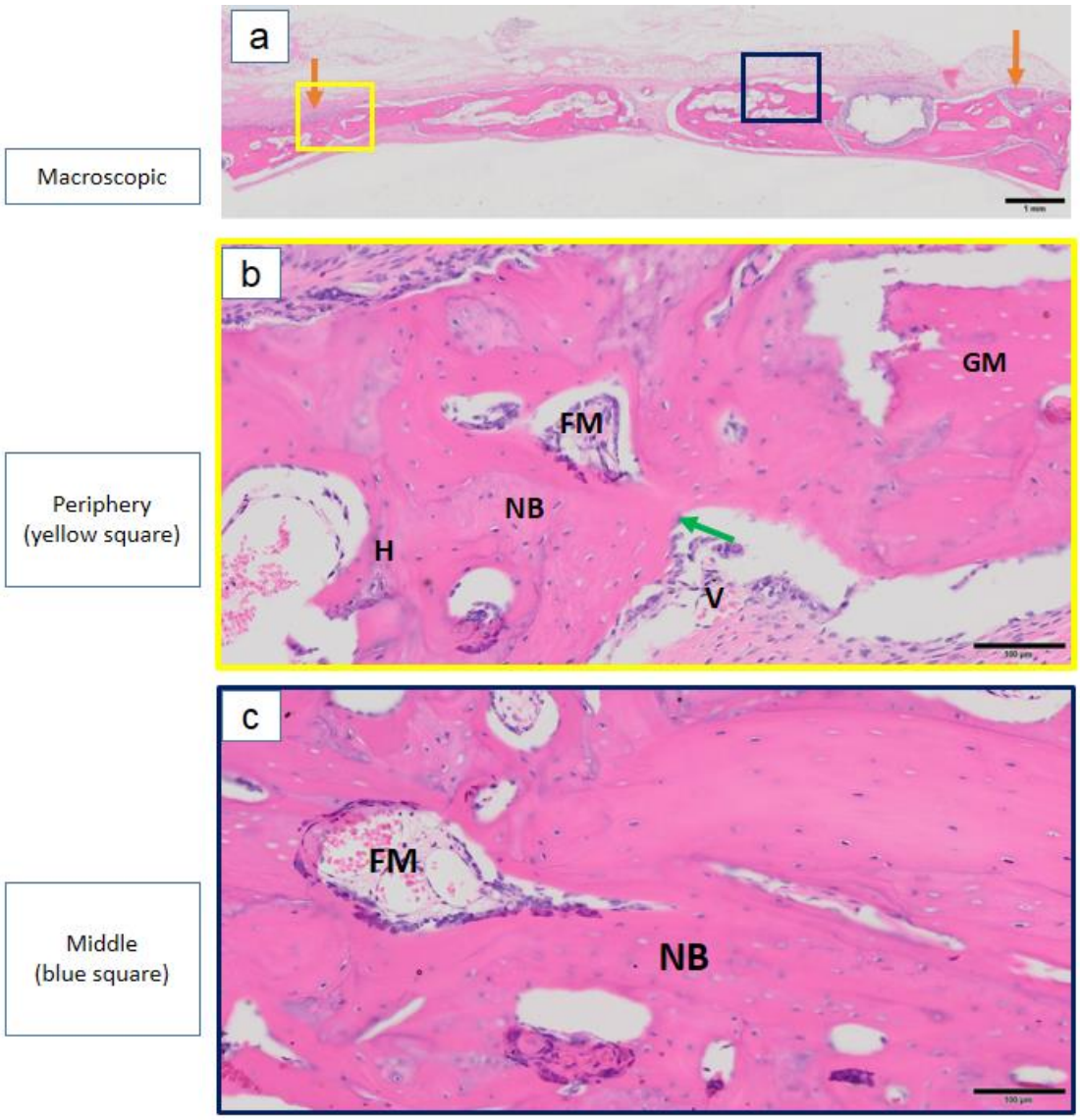

Fig. 19 The histology of the AB group at 4 weeks. (a) The color of graph was pink, and did not present inflammatory area within defect, scale bar= 1mm. The periphery site (yellow square) was focused at (b). The middle site (blue square) was focused at (c). Scale bars: 100μm. H : host bone, NB: new bone, V: vascula, GM: residual graft material, FM: fatty bone marrow, Orange arrow: the margin of the defect and host bone, Green arrow: osteoblast.

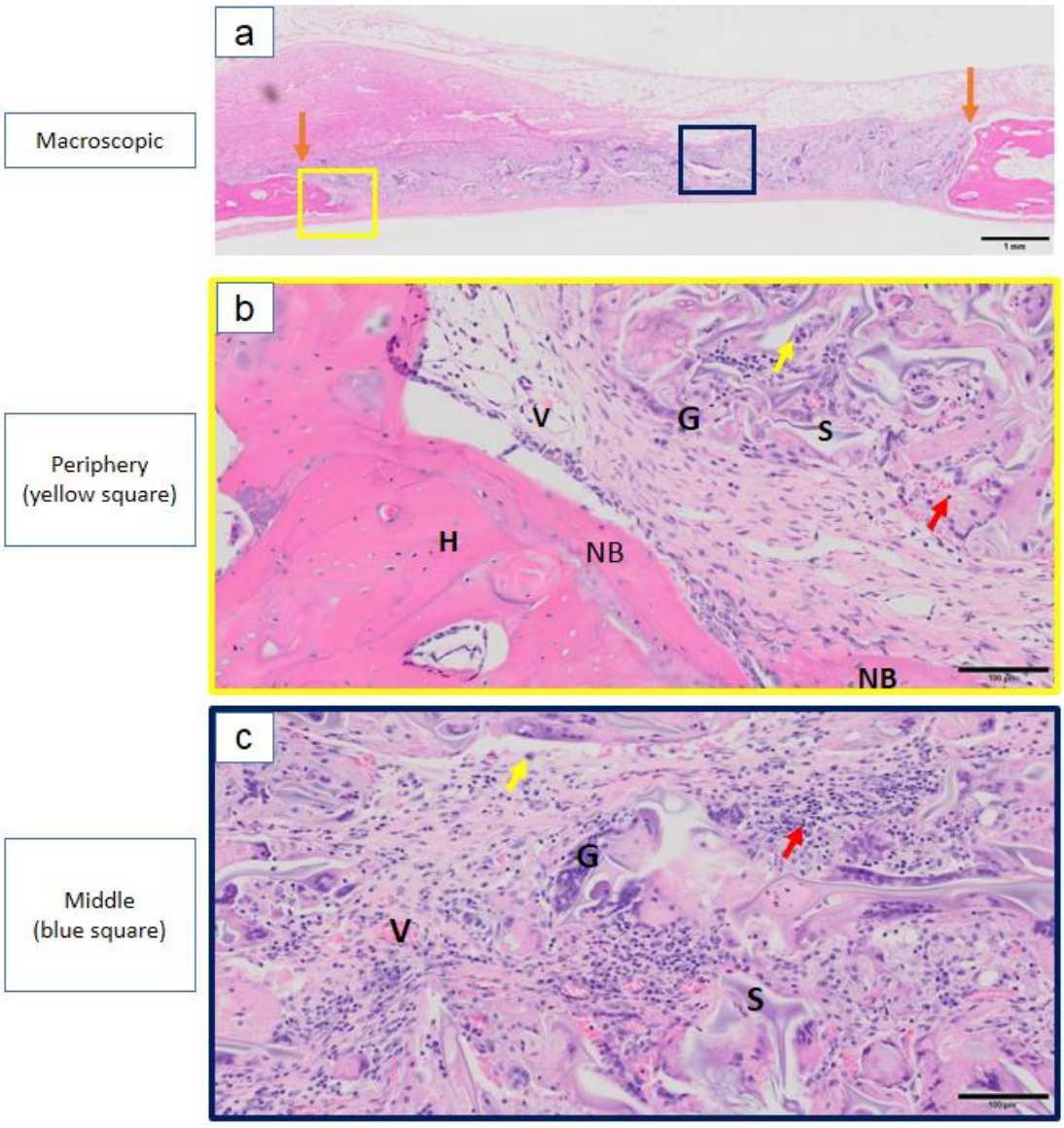

Fig. 20 The histology of the SF group at 4 weeks. (a) The implant collapsed, and was inhomogenous purple color. scale bar= 1mm. The periphery (yellow square) was focused at (b). The middle site (blue square) was focused at (c). Scale bars: 100μm. H: host bone, NB: new bone, V: vascula, S: residual silk material, G: foreign-body giant cells, Orange arrow: the margin of the defect and host bone, Yellow arrow: macrophage, Red arrow: inflammatory cells.

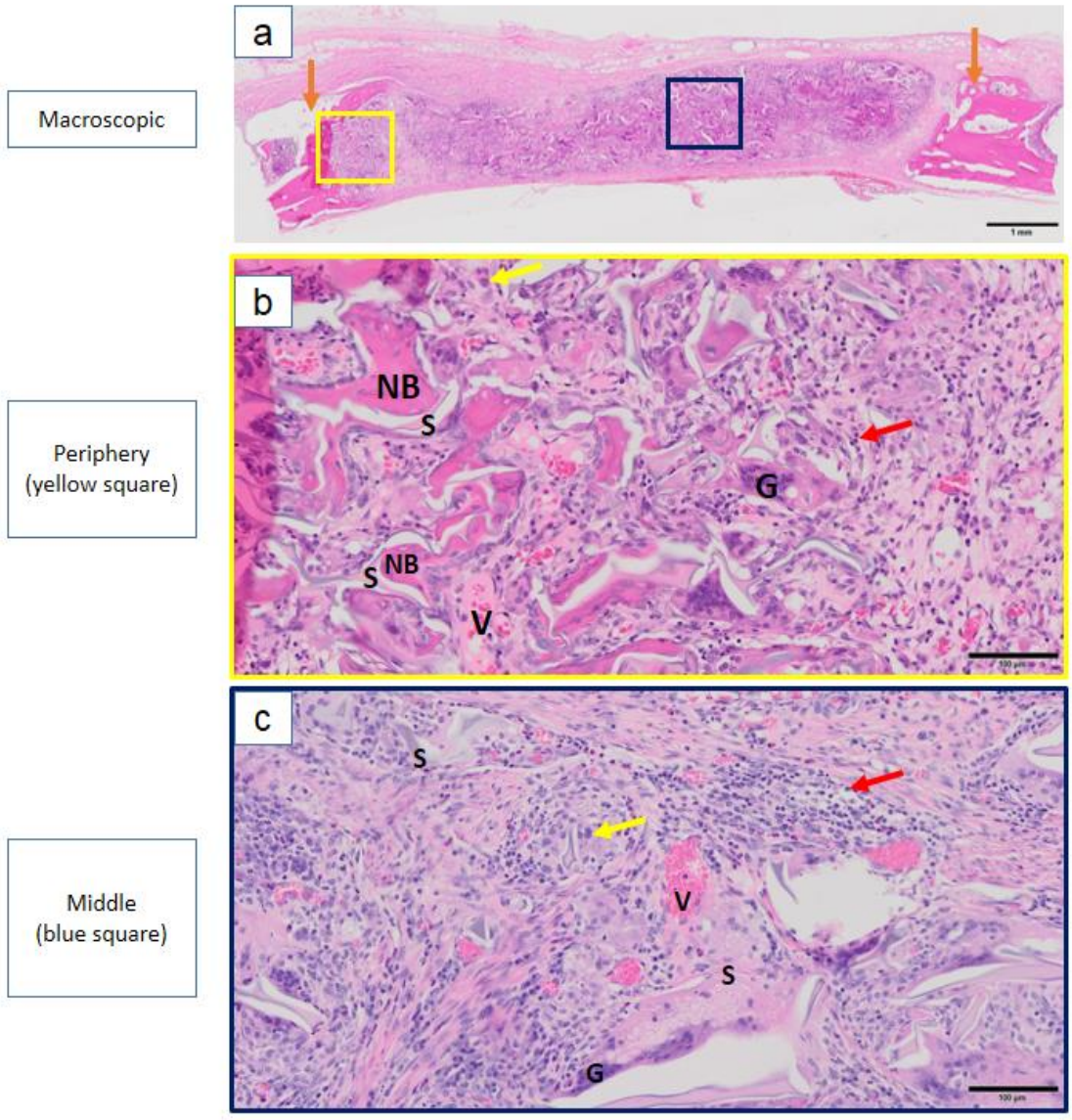

Fig. 21 The histology of the SF-FP group at 4 weeks. (a) The implant did not collapse, normal size, new bone formation enhanced among silk fibroin scaffold, scale bar= 1mm. The periphery site (yellow square) was focused at (b). The middle site (blue square) was focused at (c). Scale bars: 100µm. H: host bone, NB: new bone, V: vascula, S: residual silk material, G: foreign-body giant cells, Orange arrow: the margin of the defect and host bone, Yellow arrow: macrophage, Red arrow: inflammatory cells.

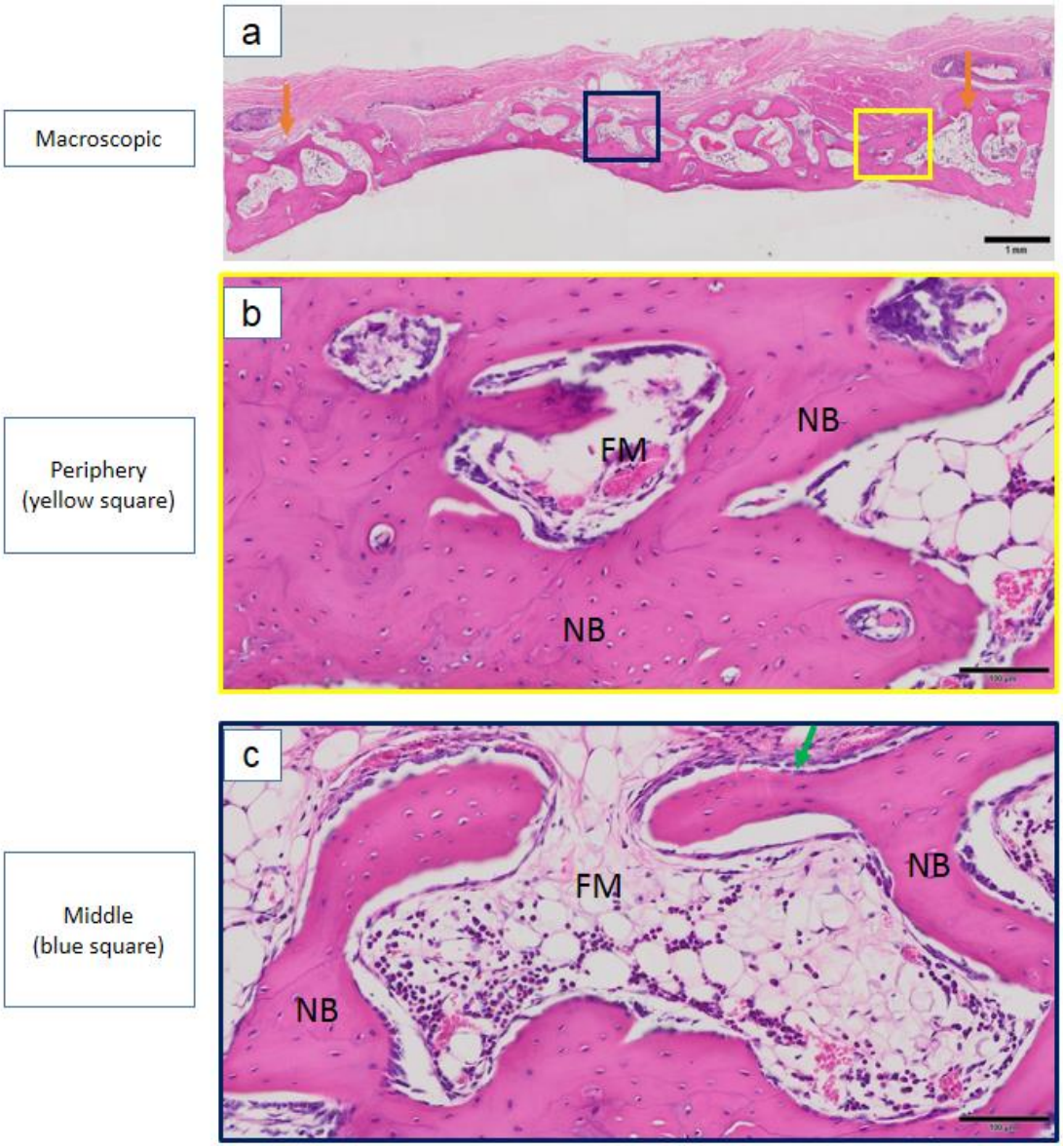

Fig. 22 The histology of the AB group at 8 weeks. (A) The implant and host bone were homogenous pink, and not presented inflammatory area, the thickness of grafting defect slightly decreased. The periphery (yellow square) was focused at (b). The middle site (blue square) was focused at (c). Scale bars: 100μm. NB: new bone, FM: fatty bone marrow, Orange arrow: the margin of the defect and host bone, Green arrow: Osteoblast.

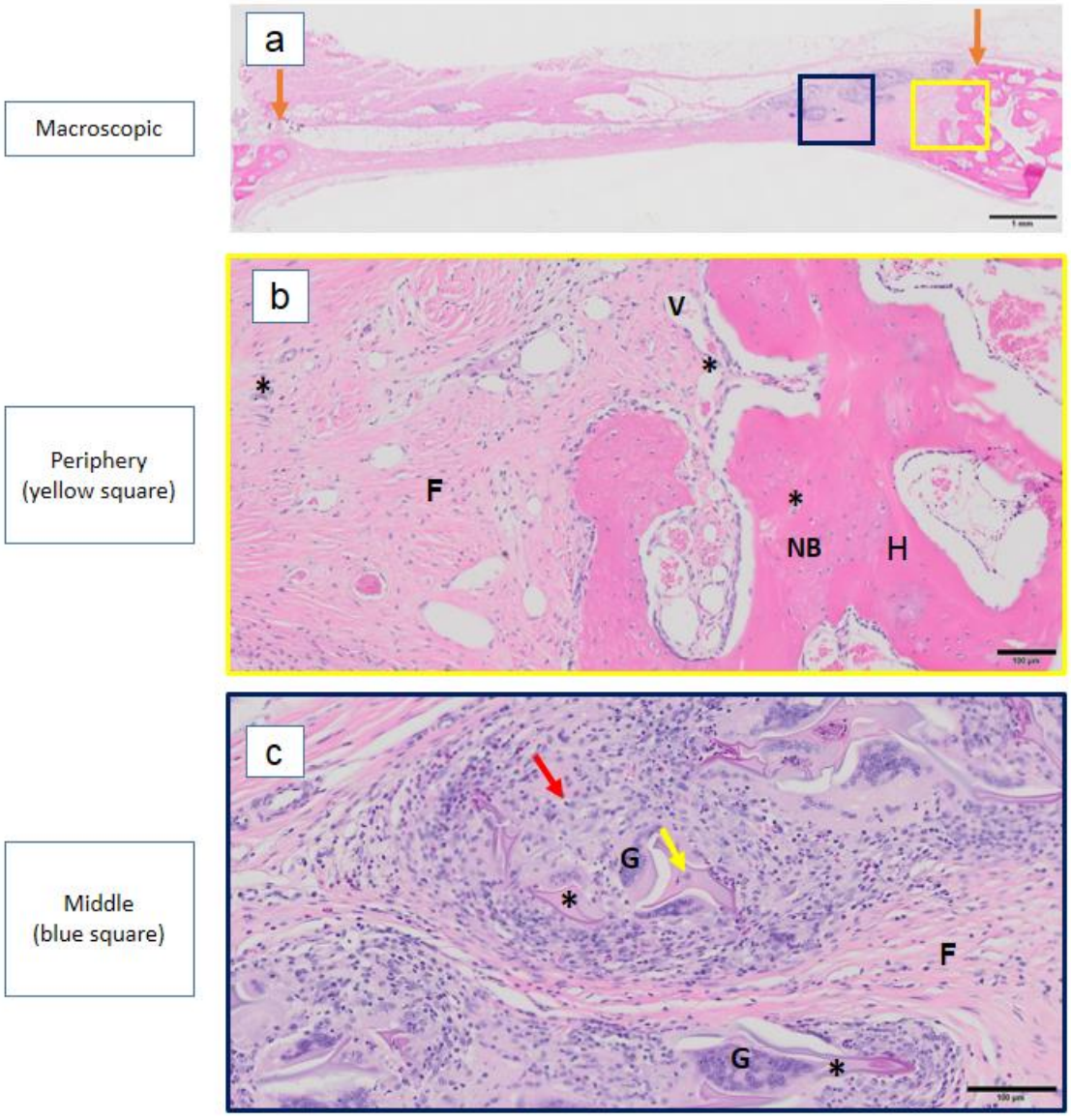

Fig. 23 The histology of the SF group at 8 weeks. (a) The implant collapsed, non-mature new bone formation enhanced around residual silk, the fibrous tissue increased at the defect. scale bar= 1mm. The periphery site (yellow square) was focused at (b). At the middle site (blue square) was focused at (c). Scale bars: 100μm. H: host bone, NB : new bone, V: vascula, G: foreign-body giant cells, F: fibrous tissue, Orange arrow: the margin of the defect and host bone, Yellow arrow: macrophage, Red arrow: inflammatory cell, *: residual silk.

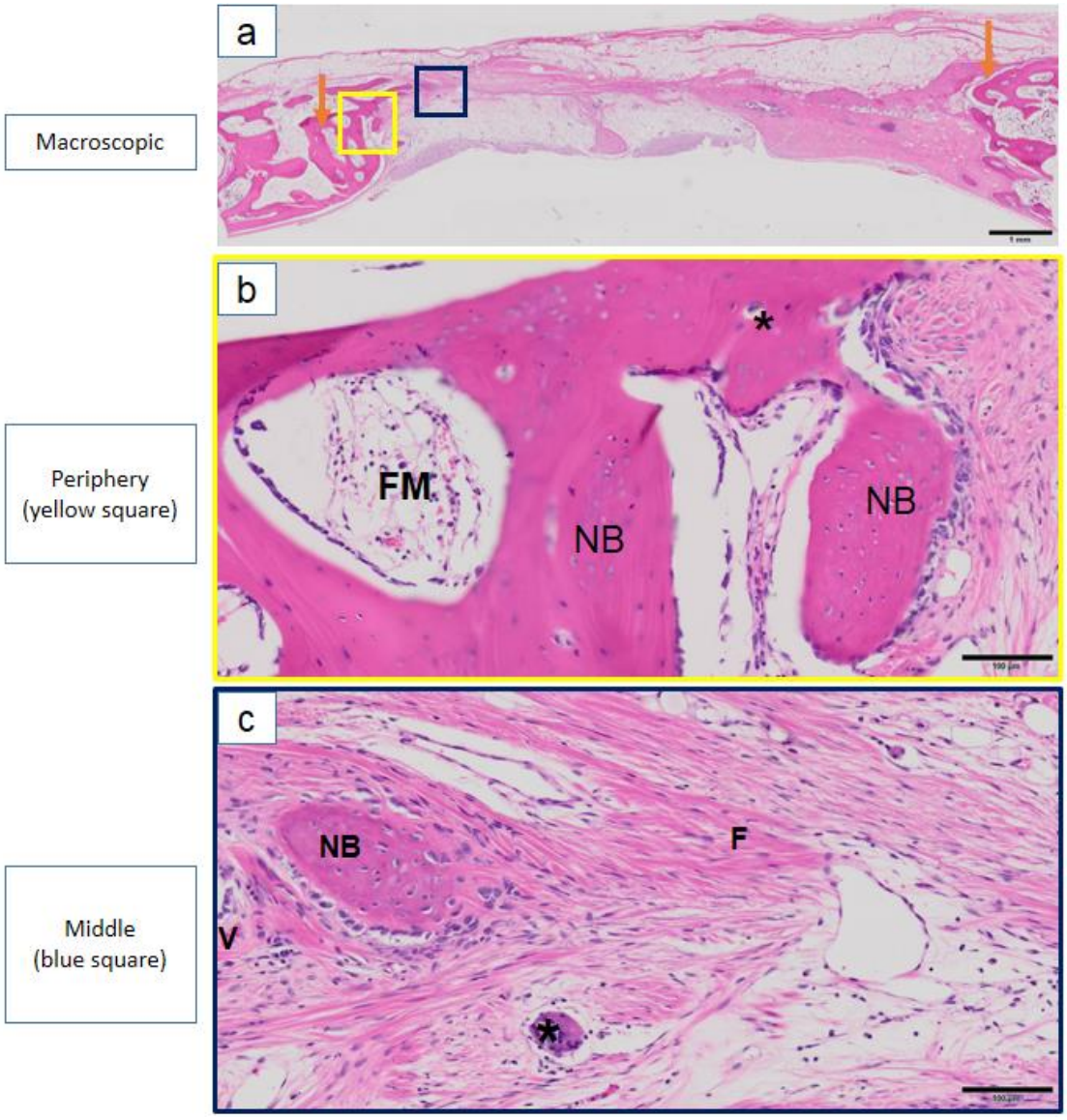

Fig. 24 The histology of the SF-FP group at 8 weeks. (a) The implant collapsed, new bone formation enhanced around residual silk more pink than 4 weeks, fibrous tissue increased at the middle. scale bar= 1mm. The periphery site (yellow square) was focused at (b). The middle site (blue square) was focused at (c). Scale bars: 100μm. H: host bone, NB : new bone, V: vascula, F: fibrous tissue, Orange arrow: the margin of the defect and host bone, Yellow arrow: macrophage, Red arrow: inflammatory cell, *: residual silk material.

Chapter 5

Discussion

One of the purposes of tissue engineering is able to design a proper scaffold to serve as a tissue structure [2]. Osteoconduction is one of the main elements in forming a scaffold for bone regeneration. The silk fibroin scaffold, which is able to encourage dependent cells attachment and development by its porosity, is a novel construction for bone generation. The other silk properties are biocompatibility, biodegradability and mechanical properties making the silk fibroin scaffold as a promising scaffold [29, 35, 53].

Materials

In this study, the SF-FP scaffolds had many particles and fibrils attaching on their walls (Fig. 9). The fibrils were enhanced by decellularized dental pulp [47]. They combined with the silk fibroin scaffolds enhanced the fibrin network artificially which encouraged to become a collagenous bone matrix. The matrix enhanced osteoblast attachment and development on the experimental scaffolds [54]. The silk fibroin scaffolds decreased their pore sizes and percent porosity after being coated with the fibronectin and decellularized dental pulp. The pore sizes of the SF-FP scaffolds were smaller than the SF scaffolds significantly ($P < 0.001$) but the porosity of the SF-FP scaffolds was only slightly different from the SF scaffolds (Table 4). Previous studies reported that the pore sizes should be at least 50 μm to permit bone growth into an artificial scaffold from *in vivo* experiments. The internal connective porosity is more important for successful anchorage bone growth than the overall pore diameter [53, 55]. Those studies support the porous features of the scaffolds of this study for bone regeneration.

The rabbit experiment models were used in the present study because they are very popular and appropriate by the following reasons. First, its bone biology is similar with human bone. Second, the rabbit’s calvarium is plate that can be

performed a uniform circular defect and can be evaluated such as radiograph and histology easily. Third, the calvarial size make the surgical procedure and specimens handling easier; Fourth, the rabbit can be placed on table without fixation; Fifth, the experimental observation is not too long follow-up because of the short life span; Finally, it is more economic, ethic than dog, pig, or sheep [56]. Moreover, the critical-size defect of the rabbit calvarium in the present study is 10 mm diameter for testing bone substitute biomaterials, it is larger than 8 mm diameter that cannot heal spontaneously throughout lifetime [57]. The postoperative time points of this study correspond with the bone healing phase response, such as inflammatory response, bone merging, quantity of bone regeneration, material resorption, etc. The lifespan of rabbits is 3-time shorter, and 3-time bone metabolism faster than human [56]. The 2 weeks and 4weeks postoperative time points are chosen to evaluate the first phase of bone healing response, such as the host reaction, the survival transplantation, the formation of new osteoid, and the immediate increase in graft radio capacity. Furthermore, the second phase of the bone healing was examined at 8 weeks to evaluate bone incorporation, bone reorganization, resorption of the experimental materials, and bone modeling [52].

Clinical healing and gross specimens

The calvaria of the rabbits in the experimental scaffolds showed good healing and the hair grew as normal (Fig. 10). Furthermore, there was no evidence of infection or wound dehiscence. The surfaces of the specimens were smooth and the colors of the specimen membranes were similar with the host. Consequently, the SF and SF-FP scaffolds had the biocompatibility property. The silk fibroin is compatible after the sericin has been extracted to decrease extreme inflammatory response [22]. Moreover, the SF-FP scaffolds did not swell as much as the SF scaffolds (Fig. 11). The decellularizing method extracted cells that made the extracellular matrix more compatible with the host in the experiments. Therefore, the host reacted successfully to the materials that indicated a clinical application of the experimental materials [58]. The critical-size defects of a few of the SF-FP and SF implants were smaller than 10-mm at the 2- and 4-week postoperative time points in this study. Additionally, they

had a rubbery consistency. They had increased stiffness at 8 weeks but only at the peripheral sites. The process of bone healing in the SF and SF-FP implants is similar with three steps of normal bone healing process. First, the bone extracellular matrix is manufactured at implants. Second, the bone formation increases its strength by mineralization. Third, bone remodeling occurs due to the resorption and reformation process [59]. Logically, the defects were still rubbery because the bone extracellular matrix had a small capacity for mineralization at 2 and 4 weeks postoperatively. In this study, the steadiness increased at 8 weeks. The bone formation was similar to the bone healing phases although it was generated at the peripheral sites.

Radiography evaluation

The 2D radiographs were taken by the digital X-ray system in the present study. The digital radiograph is better than the conventional X-ray radiography process by quality radiograph, correction of calibration, save environment, and procedure easily. The radiography results showed that the radiopacity of the SF and SF-FP groups increased at the periphery at all postoperative time points (Fig. 14). The radiopaque areas in the SF-FP group increased gradually at the peripheral defects at 2 and 4 weeks. At 8 weeks postoperatively, the radiopaque of the SF-FP group developed and moved further to the center of the defects. It indicated that the SF-FP scaffolds enhanced new bone formation better than the SF group. The AB group was high radiopaque in defects at 2 weeks, and absorbed gradually as same as bone outside defect at 4 weeks, 8 weeks at 50%, and 100%, respectively. The bone formation of the AB group was faster than the experimental groups. The modeling and remodeling process occurred during the postoperative time points [59]. Additionally the mean OD of the control group decreased gradually from 2 weeks to 8 weeks while evaluated by imaging densitometer (Table 5). The mean OD results were analyzed by digital data in two-dimensional (2D) format. The digital gray scale range is 0-255 which directly evaluates the intensity of the region of interest on a monitor. The mean OD is evaluated within the region of interest or the measured frame. In the present study, the mean OD of the SF-FP group was higher than the SF group. The gradual decreasing of the SF-FP group’s new bone formation possibly remodeled faster than the SF group.

Although we standardized our process and decreased the error effects by the digital sensor and digital software, the OD analysis still has limitations. The results affected by following reasons, such as only evaluating in 2D, error processing, technique effects of each radiographs, and image quality. Moreover, the 2D radiographs cannot evaluate bone quality and quantity such as bone volume, bone structures, and mineral bone density.

Micro-CT evaluation

The micro-CT with 3D reconstruction is the advanced method in radiography evaluation. It is able to reconstruct 3D images and evaluate 3D density and the bone mineral content. The specimens are evaluated noninvasively in a faster approach and can calculate new bone quantity. The specimens do not require the histological preparation process that includes paraffin embedding, section cutting and chemical staining [60]. In this study, the bone formation was seen clearly in the 3D reconstructed images. The defects were grafted by SF scaffolds that induced new bone at the peripheral areas of the defects (Fig. 15). New bone formation grew steadily from 2 weeks to 8 weeks postoperatively. The SF-FP implants induced new bone formation and better density than the SF implants at the periphery at 2 weeks. The new bone formation increased its quality at 4 weeks then enhanced new bone toward the center of the defect at 8 weeks postoperatively. The SF-FP scaffold enhanced more bone than in the SF group and the bone grew faster than in the SF group. It was indicated by the bone volume, trabecular thickness and bone mineral content in the micro-CT analysis. The bone volume percent of the SF-FP group was higher than in the SF group (Table 6). Moreover, the trabecular thickness structure in the SF-FP group was higher than in the SF group (Table 7). At 4 weeks, the trabecular thickness in the SF-FP group was significantly different from in the SF group ($p<0.05$). The trabecular structure of the SF-FP group was better than the SF group at the 4-week postoperative time point. However, the thickness in the SF-FP group may have decreased due to the remodeling process at 8 weeks postoperatively. The bone mineral density of the SF and SF-FP groups was growth from 2 weeks to 4 weeks and then it declined at 8 weeks postoperatively (Table 8). They were not significantly different, but importantly the

mineralization in the SF-FP group was better than in the SF group at all postoperative time points. The AB experiments were healed gradually at 2-week, 4-week, and filled completely at 8-week postoperative as the bone healing phases process. Significantly, the AB group was higher than the experimental groups in all evaluation of bone volume, trabecular thickness and bone mineral density.

Histological evaluation

The conventional histological procedure was used in the present study. The specimens were passed the decalcified process, series cutting, and H&E staining to evaluate inflammatory reaction, new bone formation, and vascular regeneration. The bone graft healing process was clearly by the healing of AB group. The phase I of the bone healing was detected at 2 weeks (Fig. 16), the 4 weeks postoperative was as a transitional process (Fig. 19), the phase II was at 8 weeks (Fig. 22).

At 2 weeks postoperatively, the defect with the SF scaffold swelled and a homogenous purple color was detected at the filled defect. New bone formation was observed at the periphery (Fig. 17). Further, the foreign-body giant cells, inflammatory cells filled the defect. Blood vessels were rarely within the SF implants. However, the SF-FP group had a better response from host at the same postoperative time points (Fig. 18). The color was pink and not dark purple as in the SF group. New bone formation was detected at the peripheral sites but it was irregular and not connected. At the middle of the SF-FP scaffolds, new bone formation was not detected but there was much blood vessels, few foreign-body giant cells and few inflammatory cells. In the first phase of bone healing in the craniofacial region, the coating components in the SF-FP group did not trigger an inflammatory response and were more biocompatible. In addition, most of the new irregular bone or woven bone was induced from the periphery where the mesenchymal cells were encouraged for recruitment in the process of intramembranous ossification. The woven bone needs more nutrition for mineralization for maturity[59].

At the 4-week postoperative time point in the SF group, it did not swell in the overall shape and the color turned pinker compared to the 2-week time point but the thickness had decreased slightly. There was new bone formation only at the

peripheral sites which did not enhance further from the margins (Fig. 19). On the other hand, the SF-FP scaffold maintained its thickness (Fig. 21). New bone formation occurred at the peripheral sites with a small amount of residual scaffold inside the new bone formation and new bone formation was enhanced further from the peripheral margin. The SF-FP clearly had osteoinductive properties since it could induce new bone formation within the silk scaffold. Since the coating solution only coated the SF-FP scaffolds, there was no new bone formation in the middle of the implant which was the same result as the SF scaffold. Moreover, vascularization in the SF-FP group was induced more than in the SF group. Vascularization is an important event for bone regeneration. It supports many essential components in bone formation, such as blood cells, oxygen, minerals and growth factors [59].

At 8 weeks postoperatively, the SF and SF-FP scaffolds collapsed at the middle and did not maintain their normal size (Fig. 23, Fig. 24). At the peripheral areas of the defects, bone formation in the SF-FP group was lamellar bone that was more mature than in the SF group. Additionally, new bone formation in the SF-FP group was enhanced forward to the center of the defect from the peripheral margin. Better vascularization encouraged new bone formation in the SF-FP group. However, the fibrous tissue, less residual scaffold and fewer inflammatory cells were detected at the middle of the site in both experimental scaffolds. These scaffolds could degrade rapidly throughout the experiment. A previous study showed that the degradation of silk fibroin scaffolds may require 1-2 years from an in vivo experiment [22].

This *in vivo* study showed that the SF scaffold had biocompatibility and the coating components made the SF scaffolds more compatible than non-coated. The decellularized dental pulp used for coating in this *in vivo* experiment not only lowered the inflammatory response but also induced more bone formation. The fabrication procedure of the decellularized component was a key character in the host reaction [58]. The ECM microenvironment of this study demonstrated that the collagenase method was the proper procedure to decellularize the dental pulp. In addition, the biological signals of the decellularized dental pulp possibly encouraged the osteoconductive property within the scaffolds to enhance new bone formation in the SF-FP group for modeling faster than in the SF group. A previous study showed that

silk fibroin scaffold combined with the sequence of fibronectin exhibited a small inflammatory reaction and fewer foreign body cells. Moreover, the decrease of the inflammatory response was assisted by vascular enhancement within the scaffold properly [13]. Besides that, the kind of inflammatory response in the SF-FP group caused slower degradation of the silk fibroin scaffold as formerly reported [61]. Furthermore, Kuboyama et al. demonstrated that the property of the scaffold's morphological surface would influence to cell development, osteoblast transformation, and bone regeneration [8].

Chapter 6

Conclusion

The coating components made the SF scaffolds were smaller pores, thicker boundary. They improved small fibrils and particles at the porous structures.

Furthermore, the SF-FP scaffolds demonstrated that there were low inflammation and well growth of bone and vascular tissue formation at those bone defects. Therefore, the SF-FP scaffolds are the good biocompatibility and vascular regeneration characteristics.

The silk fibroin scaffolds coated with fibronectin and decellularized dental pulp enhanced new bone formation in rabbit calvaria defects. The results indicate that the SF-FP scaffolds have the new bone formation functionality; to enhance bone density, bone volume fraction at bone defect area of rabbit calvaria. The SF-FP is good osteoconductive property, and enhance osteoinductive bone cells.

Moreover, the SF-FP scaffolds had the degradation property. They decreased their representation in the experiment period. They could not maintain their thickness at the end of the sacrifice time point by degradable.

Finally, this study exhibited that the coating silk fibroin scaffolds coated with fibronectin and decellularized dental pulp may promise to use as a novel bone scaffold for bone tissue engineering.

References

1. Garg AK. ***Bone biology, harvesting and grafting for dental implants: rationale and clinical applications***. Quintessence Publishing Company; 2004.
2. Antonio J. Salgado OPC, Rui L. Reis. Bone Tissue Engineering: State of the Art and Future Trends. ***Macromol Biosci.*** 2004(4):743-65.
3. Langer R, Vacanti JP. Tissue engineering. ***Science***. 1993;260(5110):920-6.
4. Felicity R. A. J. Rose ROCO. Bone Tissue Engineering: Hope vs Hype. ***Biochem Biophys Res Commun.*** 2002(292):1-7.
5. Ma PX. Scaffolds for tissue fabrication. ***Materials Today***. 2004.
6. Kundu B, Rajkhowa R, Kundu SC, Wang X. Silk fibroin biomaterials for tissue regenerations. ***Adv Drug Deliv Rev***. 2013;65(4):457-70.
7. Biman B. Mandal, Ariela Grinberg, Eun Seok Gil, Bruce Panilaitis, Kaplan DL. High-strength silk protein scaffolds for bone repair. ***Proc Natl Acad Sci***. 2012(109):7699-704.
8. Kuboyama N, Kiba H, Arai K, Uchida R, Tanimoto Y, Bhawal UK et al. Silk fibroin-based scaffolds for bone regeneration. ***J Biomed Mater Res B Appl Biomater***. 2013;101(2):295-302.
9. Wohlrab S, Muller S, Schmidt A, Neubauer S, Kessler H, Leal-Egana A et al. Cell adhesion and proliferation on RGD-modified recombinant spider silk proteins. ***Biomaterials***. 2012;33(28):6650-9.
10. Lee EH, Kim JY, Kweon HY, Jo YY, Min SK, Park YW et al. A combination graft of low-molecular-weight silk fibroin with Choukroun platelet-rich fibrin for rabbit calvarial defect. ***Oral Surg Oral Med Oral Pathol Oral Radiol Endod.*** 2010;109(5):e33-8.
11. Badylak SF. Xenogeneic extracellular matrix as a scaffold for tissue reconstruction. ***Transpl. Immunol.*** 2004;12(3–4):367-77.
12. Xu J, Mosher D. Fibronectin and Other Adhesive Glycoproteins. In: Mecham RP, editor. The Extracellular Matrix: an Overview. ***Biology of Extracellular Matrix.*** Springer Berlin Heidelberg; 2011. p. 41-75.

13. Hofmann S, Hilbe M, Fajardo RJ, Hagenmüller H, Nuss K, Arras M et al. Remodeling of tissue-engineered bone structures in vivo. ***Eur J Pharm Biopharm***. 2013;85(1):119-29.
14. Crapo PM, Gilbert TW, Badylak SF. An overview of tissue and whole organ decellularization processes. ***Biomaterials***. 2011;32(12):3233-43.
15. Lutolf MP, Hubbell JA. Synthetic biomaterials as instructive extracellular microenvironments for morphogenesis in tissue engineering. ***Nat Biotech.*** 2005;23(1):47-55.
16. Salvay DM, Rives CB, Zhang X, Chen F, Kaufman DB, Lowe WL, Jr. et al. Extracellular matrix protein-coated scaffolds promote the reversal of diabetes after extrahepatic islet transplantation. ***Transplantation***. 2008;85(10):1456-64.
17. Goldberg M, Smith AJ. Cells and Extracellular Matrices of Dentin and Pulp: A Biological Basis for Repair and Tissue Engineering. ***Crit Rev Oral Biol Med.*** 2004;15(1):13-27.
18. Sangkert S, Kamonmattayakul S, Chai WL, Meesane J. A biofunctional-modified silk fibroin scaffold with mimic reconstructed extracellular matrix of decellularized pulp/collagen/fibronectin for bone tissue engineering in alveolar bone resorption. ***Materials Letters.*** 2016;166:30-4.
19. Thomas J. Cypher JPG. Biological Principles of Bone Graft Healing. ***J Foot Ankle Surg.*** 1996;35(5):413-7.
20. G. Daculsi BHF, T. Miramonda, M. Durand. Osteoconduction, Osteogenicity, Osteoinduction, what are the fundamental properties for a smart bone substitutes. ***IRBM***. 2013(34):346–8.
21. O'Brien FJ. Biomaterials & scaffolds for tissue engineering. ***Materials Today***. 2011;14(3):88-95.
22. Altman GH, Diaz F, Jakuba C, Calabro T, Horan RL, Chen J et al. Silk-based biomaterials. ***Biomaterials***. 2003;24(3):401-16.
23. Fiorenzo G. Omenetto DLK. New Opportunities for an Ancient Material. ***Science***. 2010;329(5991):528-31.

24. MA B, G A, S Z, MA B. The enhancement of osteoblast growth and differentiation in vitro on a peptide hydrogel-polyHIPE polymer hybrid material. ***Biomaterials.*** 2005;26:5198.
25. Goddard JM, Hotchkiss JH. Polymer surface modification for the attachment of bioactive compounds. ***Prog. Polym. Sci.*** 2007;32(7):698-725.
26. Chang H-I, Wang Y. Cell responses to surface and architecture of tissue engineering scaffolds. ***INTECH Open Access Publisher***; 2011.
27. Horan RL, Antle K, Collette AL, Wang Y, Huang J, Moreau JE et al. In vitro degradation of silk fibroin. ***Biomaterials***. 2005;26(17):3385-93.
28. Meinel L, Betz O, Fajardo R, Hofmann S, Nazarian A, Cory E et al. Silk based biomaterials to heal critical sized femur defects. ***Bone***. 2006;39(4):922-31.
29. Meinel L, Fajardo R, Hofmann S, Langer R, Chen J, Snyder B et al. Silk implants for the healing of critical size bone defects. ***Bone***. 2005;37(5):688-98.
30. Meinel L, Kaplan DL. Silk constructs for delivery of musculoskeletal therapeutics. ***Adv Drug Deliv Rev***. 2012;64(12):1111-22.
31. Wang Y, Rudym DD, Walsh A, Abrahamsen L, Kim H-J, Kim HS et al. In vivo degradation of three-dimensional silk fibroin scaffolds. ***Biomaterials***. 2008;29(24–25):3415-28.
32. Rockwood DN, Preda RC, Yucel T, Wang X, Lovett ML, Kaplan DL. Materials fabrication from Bombyx mori silk fibroin. ***Nat Protocols***. 2011;6(10):1612-31.
33. Santin M, Motta A, Freddi G, Cannas M. In vitro evaluation of the inflammatory potential of the silk fibroin. ***J Biomed. Mater. Res.*** 1999;46(3):382-9.
34. Hu X, Kaplan D, Cebe P. Dynamic Protein−Water Relationships during β-Sheet Formation. ***Macromolecules***. 2008;41(11):3939-48.
35. Meinel L, Hofmann S, Karageorgiou V, Kirker-Head C, McCool J, Gronowicz G et al. The inflammatory responses to silk films in vitro and in vivo. ***Biomaterials***. 2005;26(2):147-55.
36. Vepari C, Kaplan DL. Silk as a Biomaterial. ***Prog. Polym. Sci.*** 2007;32(8-9):991-1007.
37. Numata K, Cebe P, Kaplan DL. Mechanism of Enzymatic Degradation of Beta-sheet Crystals. ***Biomaterials***. 2010;31(10):2926.

38. Miyamoto S, Kathz B-Z, Lafrenie RM, Yamada KM. Fibronectin and Integrins in Cell Adhesion, Signaling, and Morphogenesis. ***Ann. N. Y. Acad. Sci.*** 1998;857(1):119-29.
39. Couchman JR, Austria MR, Woods A. Fibronectin-Cell Interactions. ***J Investig Dermatol.*** 1990;94(s6):7s-14s.
40. Sottile J, Hocking DC, Swiatek PJ. Fibronectin matrix assembly enhances adhesion-dependent cell growth. ***J Cell Sci.*** 1998;111 (Pt 19):2933-43.
41. Bini E, Foo CW, Huang J, Karageorgiou V, Kitchel B, Kaplan DL. RGD-functionalized bioengineered spider dragline silk biomaterial. ***Biomacromolecules***. 2006;7(11):3139-45.
42. Elkarargy A. Biological functionalization of dental implants with fibronectin: a scanning electron microscopic study. ***Int. J Health Sci.*** 2014;8(1):57-66.
43. Hinderer S, Layland SL, Schenke-Layland K. ECM and ECM-like materials — Biomaterials for applications in regenerative medicine and cancer therapy. ***Adv. Drug Deliv Rev.*** 2016;97:260-9.
44. Benders KEM, Weeren PRv, Badylak SF, Saris DBF, Dhert WJA, Malda J. Extracellular matrix scaffolds for cartilage and bone regeneration. ***Trends Biotechnol.*** 2013;31(3):169-76.
45. Linde A. The extracellular matrix of the dental pulp and dentin. . ***J. Dent. Res.*** 1985;64 Spec No:523-9.
46. Traphagen SB, Fourligas N, Xylas JF, Sengupta S, Kaplan DL, Georgakoudi I et al. Characterization of natural, decellularized and reseeded porcine tooth bud matrices. ***Biomaterials***. 2012;33(21):5287-96.
47. Sangkert S, Meesane J, Kamonmattayakul S, Chai WL. Modified silk fibroin scaffolds with collagen/decellularized pulp for bone tissue engineering in cleft palate: Morphological structures and biofunctionalities. ***Mat Sci. Eng. C Mater. Biol Appl***. 2016;58:1138-49.
48. Chang G, Kim HJ, Kaplan D, Vunjak-Novakovic G, Kandel RA. Porous silk scaffolds can be used for tissue engineering annulus fibrosus. ***Eur Spine J***. 2007;16(11):1848-57.

49. Correia C, Bhumiratana S, Yan LP, Oliveira AL, Gimble JM, Rockwood D et al. Development of silk-based scaffolds for tissue engineering of bone from human adipose-derived stem cells. ***Acta Biomater.*** 2012;8(7):2483-92.
50. Yong Zhao, R. Z Legeros, Chen aJ. Initial Study on 3D Porous Silk Fibroin Scaffold: Preparation and Morphology. ***Ashdin Publishing Bioceramics Development and Applications***. 2011;1.
51. Manjeet Mapara BST, and K. M. Bhat. Rabbit as an animal model for experimental research. ***Dent Res J (Isfahan)***. 2012;9 (1):111–8.
52. Pearce AI, Richards RG, Milz S, Schneider E, Pearce SG. Animal models for implant biomaterial research in bone: a review. ***Eur. Cell Mater.*** 2007;13:1-10.
53. Uebersax L, Apfel T, Nuss KM, Vogt R, Kim HY, Meinel L et al. Biocompatibility and osteoconduction of macroporous silk fibroin implants in cortical defects in sheep. ***Eur. J. Pharm. Biopharm.*** 2013;85(1):107-18.
54. Mavrogenis AF, Dimitriou R, Parvizi J, Babis GC. Biology of implant osseointegration. ***J. Musculoskelet. Neuronal Interact***. 2009;9(2):61-71.
55. Hollister SJ. Scaffold Design and Manufacturing: From Concept to Clinic. ***Adv. Mater.*** 2009;21(32-33):3330-42.
56. Michael IS, Mark PM. Animal Models for Bone Tissue Engineering of Critical-sized Defects (CSDs), Bone Pathologies, and Orthopedic Disease States. ***Bone Tissue Engineering***. CRC Press; 2004. p. 217-44.
57. Sohn J-Y, Park J-C, Um Y-J, Jung U-W, Kim C-S, Cho K-S et al. Spontaneous healing capacity of rabbit cranial defects of various sizes. ***J Periodontal Implant Sci.*** 2010;40(4):180-7.
58. Stephen F. Badylak TG. Immune response to biologic scaffold materials. ***Sem Immunol.*** 2008;20:109–16.
59. Kini U, Nandeesh BN. Physiology of Bone Formation, Remodeling, and Metabolism. In: Fogelman I, Gnanasegaran G, van der Wall H, editors. **R*adionuclide and Hybrid Bone Imaging***. Berlin, Heidelberg: Springer Berlin Heidelberg; 2012. p. 29-57.
60. Tuan H HD. Application of micro CT and computation modeling in bone tissue engineering. ***Comput. Aided Des.*** 2005; 37 1151–116.

61. Lickorish D, Chan J, Song J, Davies JE. An in-vivo model to interrogate the transition from acute to chronic inflammation. ***Eur. Cell Mater.*** 2004;8:12-9; discussion 20.

Appendix

PRINCE OF SONGKLA UNIVERSITY
15 Karnjanawanij Road, Hat Yai, Songkhla 90110, Thailand
Tel (66-74) 286958 Fax (66-74) 286961
Website : www.psu.ac.th

MOE 0521.11/ 520 Ref.07/2015

April 28 , 2015

This is to certify that the research project entitled "Evaluate new bone formation by silk fibroin scaffold coated with fibronectin and decellularized dental pulp on rabbit models" which was conducted by Assoc. Prof. Dr.Thongchai Nuntanaranont, Faculty of Dentistry, Prince of Songkla University, has been approved by The Animal Ethic Committee, Prince of Songkla University.

Kitja Sawangjaroen, Ph.D.
Chairman,
The Animal Ethic Committee, Prince of Songkla University

RESEARCH ETHICS COMMITTEE (REC)
BUILDING 1 5TH FLOOR ROOM 504
TEL. 66-74-287533, 66-74-287504
FAX. 66-74-287533

FACULTY OF DENTISTRY
PRINCE OF SONGKLA UNIVERSITY
HADYAI, SONGKHLA 90112, THAILAND
TEL. 66-74-212914, 66-74-429871, 66-74-287500
FAX. 66-74-429871, 66-74-212922

Documentary Proof of Ethical Clearance

Research Ethics Committee (REC)

Faculty of Dentistry, Prince of Songkla University

The Project Entitled Evaluation of New Bone Formation in Rabbit Calvaria Using Silk Fibroin Scaffolds Coated with Fibronectin and Decellularized Dental Pulp

REC Project No. : EC5802-03-P- HR

Principal Investigator : Mr.Thanh Huy Thai

Approved by Research Ethics Committee (REC), Faculty of Dentistry, Prince of Songkla University.

This is to certify that REC is in full Compliance with International Guidelines for Human Research Protection such as the Declaration of Helsinki, the Belmont Report, CIOMS Guidelines and the International Conference on Harmonization in Good Clinical Practice (ICH-GCP).

Date of Approval : 24 APRIL 2015 **No. of Approval** : MOE 0521.1.03/ 486

(Asst. Prof. Dr. Srisurang Suttapreyasri)
Chairman of Research Ethics Committee

(Asst. Prof.Surapong Vongvatchranon)

(Dr. Supatcharin Piwat)

(Assoc. Prof. Pornchai Sathirapanya)

(Mr. Kamolphan Nuangsri)

(Asst. Prof. Dr. Angkana Thearmontree)

(Mr. Wasin Suwannarat)

(Asst. Prof. Dr. Suwanna Jitpakdeebodintra)

(Mr. Boonsit Buaban)

Vitae

Name Mr. Thanh Huy Thai

Student ID 5710820001

Educational Attainment

Degree	Name of institutions	Year of raduation
Doctor of Dental Surgery	Can Tho University of Medicine and Pharmacy (Vietnam)	2008

Scholarship Awards During Enrolment

Thailand's Education Hub for Southern Region of ASEAN Countries (TEH-AC) Scholarship

Runner-up poster Award, presented by the 3rd Annual Symposium of the Hochiminh city Society of Dental Implant, 2015

Working Place

Can Tho Hospital of Eyes and Odonto-Stomatology, Can Tho city 900000, Vietnam.

List of Publication and Proceeding (add if Prosible)

"Evaluation of New Bone Formation Enhanced by the 3D Silk Fibroin Scaffolds in Rabbits' Calvarial Defects" in The Royal College of Dental Surgeons of Thailand Conference, 14-16 September 2016, Centara Grand at CentralWorld, Thailand.

"New Bone Regeneration Enhanced by Coated Silk Fibroin Scaffolds for Alveolar Clefts-An Animal Experiment" in 12th Asian Congress on Oral and Maxillofacial Surgery Conference, 9-12 November 2016, Manila, Philippines.